UNIVERSITY OF CALIFORNIA, SAN DIEGO

Analysis of Binding Relationships between Cys-loop Receptors and Acetylcholine Binding Protein Mutants using Selective Tropane Triazole Compounds

A Thesis submitted in partial satisfaction of the requirements for the degree

Master of Science

in

Biology

by

Bill T. Chen

Committee in charge:

Professor Palmer Taylor, Chair
Professor Nicholas Spitzer, Co-Chair
Professor Roberto Malinow

2015

The Thesis of Bill T. Chen is approved, and it is acceptable in quality and form for publication on microfilm and electronically:

_____

_____

Co-Chair

_____

Chair

University of California, San Diego

2015

DEDICATION

To my parents and friends

For their unyielding patience

EPIGRAPH

When we are not sure, we are alive.

Graham Greene

TABLE OF CONTENTS

LIST OF FIGURES

LIST OF TABLES

LIST OF ABBREVIATIONS

5-HT…..……..5-Hydroxytryptamine

ACh……..……..……..Acetylcholine

AChBP…….....……Acetylcholine Binding Protein

Ac……..……..…….*Aplysia californica*

APP……..……..……..Amyloid Precursor Protein

aCSF…..……..…….……..Artificial Cerebral Spinal Fluid

Aβ…..……Beta Amyloid

CNS……Central nervous system

DMEM……..……Dulbecco's modified Eagle's medium

FBS……Fetal bovine serum

FPLC……..……...…Fast performance liquid chromatography

GABA……..……..Gamma-aminobutyric acid

HEK…..…….……..Human embryonic kidney

LBD…..…….…….……Ligand Binding Domain

LGIC…..…….……Ligand-gated Ion Channel

LTP…..…….……...Long Term Potentiation

Ls…..…….....*Lymnaea stagnalis*

MLA…..…….……..Methyllycaconitine

nAChRs…..……...Nicotinic Acetylcholine Receptors

PNS…..…….……...Peripheral Nervous System

TM…..…….……Transmembrane Helix

Amino Acid Residues

A or Ala..……..…….Alanine

C or Cys……..……..……..Cysteine

D or Asp……..…….Asparagine

E or Glu……..……..……Glutamate

F or Phe……..……Phenylalanine

G or Gly..…….Glycine

H or His…...……..……...Histidine

I or Ile……..……..……..Isoleucine

K or Lys……..……..Lysine

L or Leu……..……Leucine

M or Met……..…….Methionine

N or Asn…...……..……..…Asparagine

P or Pro……..……..……..Proline

Q or Gln.. ……..……..……..……..……..Glutamine

R or Arg...……..……Arginine

S or Ser……..……..Serine

T or Thr……..……Threonine

V or Val……..Valine

W or Trp……..……..……..Tryptophan

Y or Tyr……..……..……..……..……Tyrosine

ACKNOWLEDGEMENTS

I would like to thank Dr. Palmer Taylor for the opportunity for me to join his lab and letting me work on the nAChR project. I would also like to thank John G. Yamauchi for being an excellent mentor and friend throughout these years. I would also like to thank the entire Taylor lab, both past and present, for their invaluable help on various aspects of the project.

ABSTRACT OF THE THESIS

Analysis of Binding Relationships between Cys-loop Receptors and Acetylcholine Binding Protein Mutants using Selective Tropane Triazole Compounds

by

Bill T. Chen

Master of Science

in

Biology

University of California, San Diego, 2015

Professor Palmer Taylor, Chair

Professor Nicholas Spitzer, Co-Chair

α7 nAChRs and 5-HT_{3A} receptors are important targets for potential theraupeutic treatments in pharmacological drug design. α7 nAChRs are implicated in CNS disorders such as Alzheimer's disease and schizophrenia, while 5-HT_{3A} receptors are targets for anti-emetic drug design. The objective of

this thesis is to identify and understand determinants that are important to α7 nAChR and 5-HT_{3A} receptor selectivity, and use these principles to develop potentially selective leads.

To accomplish this, I first looked at several potent tropane triazole compounds generated through *in situ* click-chemistry on acetylcholine binding protein templates. Close examination of the data recognized a distinct relationship between quaternary tropane amines and high potency as α7 nAChR agonists. The 5-HT_{3A} receptor was found to prefer tertiary tropane antagonists. Crystal studies using AChBP elucidated the differences in the orientation of the tropane ring in the binding pocket, leading us to understand the general selectivity the aromatic nest provides for α7 nAChR and 5-HT_{3A} receptor.

To further understand ligand selectivty at α7 nAChR and 5-HT_{3A} receptor, I mutated Aplysia californica AChBP to one a7-similar mutant and two 5-HT_{3A}-similar mutants. α7-similar mutant, Ac α7 (1), showed greater selectivity for quaternary tropanes due to its substantial loss of binding affinity for tertiary tropanes compared to wild-type *Ac*. From the 5-HT_{3A}-similar mutants, Arg 57 was found to enhance affinity of tertiary tropanes through strong cation-π interaction with the hydrophobic aromatic rings. These findings help further elucidate the critical residues in the complementary subunit that determine ligand selecitivity at α7 nAChR and 5-HT_{3A} receptors.

I

INTRODUCTION

Overview of Cys-loop receptors and their role as pharmaceutical targets for CNS diseases and disorders

Cys-loop receptors are a superfamily of pentameric ligand-gated ion channels (pLGICs) consisting of nicotinic acetylcholine receptors, 5-HT_3, glycine, γ-amino butyric acid type A (GABA-A), and other neurotransmitter receptors. These receptors are constructed of a large N-terminal extracellular ligand binding domain (LBD) consisting of 5 protein subunits that can be identical (homomeric) or composed of several variations of different subunits (heteromeric) (Bouzat, 2012). These receptors are named 'Cys-loop receptors' due to their commonality in a conserved loop of 13 residues between two Cys residues joined by disulfide bond in the LBD (Tsetlin et al., 2011). This Cys-loop rests above the transmembrane domain consisting of 4 membrane-spanning regions (M1-4) which hold the ion channel – a gated pore that, when open, allow for passive ion movement by electrochemical gradient across the membrane (Unwin, 2005). The Cys-loop is thought to be involved in receptor gating by controlling the rotation of the M2 helix and the opening of the pore.

Nicotinic acetylcholine receptors (nAChRs) are excitatory, cation-selective Cys-loop receptors that are essential for synaptic transmission in the central and peripheral nervious systems. Located in both the pre- and post-synaptic membranes, nAChRs are composed of a selection of 17 homologous polypeptides, α1-10, β1-4, γ, δ, and ε, that, through selective combination of subunits, form various unique subtypes of nAChRs. Neuronal nAChR subtypes are further divided into two cateogries: homomeric subtypes formed entirely of

α7-α9 subunits, and heteromeric subtypes containing α2-6 and β2-4 subunits. (Kalamida et al., 2007)

Among the nAChR subtypes, the α7 homomeric nAChR has shown to be a potential therapeutic target for many CNS diseases such as schizophrenia and Alzheimer's disease. Expressed at high levels in the cortex and hippocampus, the α7 receptor is a rapid-desensitizing receptor that triggers high amounts of calcium ion influx relative to heteromeric receptors (Jensen et al., 2005). Direct examination of postmortem tissue from schizophrenic patients reveals a decreased expression of α7 nAChRs in the dentate gyrus and hippocampal area CA3 as well as reduced α7 nAChR binding in the cingulate cortexes of patients (Young and Geyer, 2013). Furthermore, α7 nAChR is known to modulate dopamine, glutamate, and GABA neurotransmitters and may improve cognitive symptoms in schizophrenic patients by increasing the release of dopamine in the prefrontal cortex or modulating the activation of glutamatergic neurons to increase dopamine output in the striatum (Bencherif et al., 2012). These studies concerning the lack of binding or expression of α7 nAChRs in schizophrenic patients implicate that α7 nAChRs have an important role in the pathology of schizophrenia. In Alzheimer's studies, α7 nAChRs have also shown to have neuroprotective effects against Aβ toxicity via the P13K pathway, indicating the potential trophic effect of the α7 nAChR in treatment of Alzheimer's disease (Parri et al., 2011).

Unlike other 5-HT G-protein-coupled receptors, 5-HT_3 receptors are serotonergic, cation-selective LGICs that are part of the Cys-loop receptor family.

Similar to nAChRs and other Cys-loop receptors, 5-HT_3 receptors (5-HT_3R) are composed of 5 protein subunits that surround the ion-conducting pore in the extracellular LBD. Each subunit is also comprised of a transmembrane domain and an intracellular domain. 5-HT_3Rs are located in both the central and peripheral nervous systems, serving as neurotransmitter receptor for various sympathetic, parasympathetic, and sensor functions in the PNS. In the CNS, 5-HT_3Rs are located in many areas including the cortex, hippocampus, and substantia nigra, serving as enhancers of the release of neurotransmitters such as dopamine and GABA upon activation. Functionally, they play a role in cognitive functions as well as in emesis and anxiety. (Thompson and Lummis, 2006)

There are several identified 5-HT_3 subunits, 5-HT_{3A-E}, with the 5-HT_{3A} subunit forming either homomers or heteromers with the 5-HT_{3B} subunit. In its homopentameric form, the 5-HT_{3A} receptor is widely used as a therapeutic target in drug design for antiemetic medication, where 5-HT_{3A} receptor antagonists are developed and used for treatment of chemotherapy-induced and postoperative nausea to suppress strong instances of emesis (Lummis, 2012). 5-HT_{3A} receptor has also been implicated as a potential target for treatment of alcoholism, resulting in a decreased consumption of alcohol after treatment with 5-HT_3 antagonists (Hodge et al., 2004).

Acetylcholine-binding proteins and their role as structural and functional templates for receptor subunit interfaces

Acetylcholine-binding proteins (AChBPs) are soluble protein that are secreted by molluscan glial cells of sea hare and freshwater snail, *Aplysia californica* (*Ac*) and *Lymnea stagnalis* (*Ls*) respectively. They are stable homopentamers with 5 ligand binding sites and serve to represent as structural and functional homolog of the extracellular LBD of pLGICs such as nAChR and 5-HT_3 (Celie et al., 2004). Although they only share a 22-30% in protein identity with nAChRs and less so with other pLGICs, many residues relevant to ligand binding are conserved in the AChBP binding interface, and many known nAChR agonists and antagonists such as acteylcholine, epibatidine, nicotine, and α-bungarotoxin are capable of binding to the AChBP subunits (Brejc et al., 2001). Both *Ac* and *Ls* display the greatest similarities to α7 nAChR, showing close to 30% protein identity. (Table 5)

Crystal structures of AchBP with nicotine and subsequently epibatidine, lobeline, and methyllcaconitine (MLA) have been solved through the use of X-ray crystallography (Rucktooa et al., 2009). These crystal structures allow for further understanding of AChBP subunit interface and subsequently the subunit interfaces of nAChRs and other Cys-loop receptors. Each ligand-binding subunit interface is composed from 6 loops: loops A, B, and C from the principal subunit and loops D, E, and F from the complementary subunit. Aromatic residues from the loops interact with the ligand, forming an aromatic nest around the molecule. The aromatic nest is made up primarily by 5 aromatic residues: Tyr 93, Trp 147, Tyr 188, and Tyr 195 from the principal subunit and Tyr55 from the complementary subunit. Trp147 on loop B, present in both AChBPs, is

particularly important due to its strong contribution to ligand stabilization through both hydrogen bonding from its carbonyl oxygen and van der Waals interaction from its ethyl group with the ligand. Similarly, Tyr 55 on loop D of the complementary subunit show hydrogen bonding to the amine group of the ligand, but is present only in *Ac* AChBP. *Ac* Y55W, an *Ac* mutant with a single mutation Y55W, is used during compound screening in conjunction with wild-type AChBPs due to the residue's importance in nAChR binding. (Hansen et al., 2005) (Figure 1)

Synthesis of the 1,2,3-triazole series of compounds using *in situ* azide-alkyne click-chemistry

The 1,2,3-triazole series were synthesized through *in situ* azide-alkyne click-chemistry involving a catalyst-dependent azide-alkyne cycloaddition reaction (Figure 2). The resulting triazole ring was uncharged at physiological pH and was largely stable and resistant to degradation (Kolb and Sharpless, 2003). Furthermore, the 2,3 nitrogens were able to engage in hydrogen bond interactions with surrounding water molecules and protein residues. The method used AChBPs as protein templates, in which the peripheral orthosteric sites at the interface of primary and complementary subunits helped to stabilize and facilitate the cycloaddition reaction. This process allowed for a selection of triazole products in a conformation state specific to the bound ligand state and with a high affinity for the protein templates (Yamauchi et al., 2012). *Ls*, *Ac*, and *Ac* Y55W were the protein templates used for producing the 1,2,3-triazole

products. Altogether, a total of 395 triazole compounds were synthesized and, after extensive screening using functional and AChBP binding assays, a total of 15 triazole compounds were selected for further characterization.

II

RESULTS

1,2,3-Triazole compounds generated *in situ* with *Lymnaea stagnalis* (*Ls*), *Aplysia californica* (*Ac*), and *Aplysia californica* Y55W mutant (*Ac* Y55W) show potent functional activities with α7 nAChR and 5-HT_{3A} receptors

Initially, we looked at a series of 1,2,3-triazole compounds that were generated using azide-alkyne *in situ* click-chemistry using *Ls*, *Ac*, and *Ac* Y55W acetylcholine binding proteins (AChBPs) as templates. Cycloaddition of azide and alkyne building blocks with triazole formed the stable triazole compounds (Grimster et al., 2012). The triazole compounds were screened, and fifteen compounds were identified to be potent (K_d < 30 μM) agonists and antagonists for α7 and 5-HT_{3A} receptors using the Flex assay (Table 1). Fourteen of fifteen compounds showed agonist responses at the α7 nAChRs that were subsequently blocked by α7 antagonist, methyllycaconitine (MLA). Among them, quaternary tropane triazoles, QTPh-12 and QTIn-1, showed the highest potency (EC_{50} < 50nM) as α7 agonists. Ten of the fifteen compounds showed competitive antagonist responses at the 5-HT_{3A} receptors, shown by incubating increasing concentrations of antagonist with 5-HT_{3A} intact cell receptors and a parallel shift of the Schild dose-response curve (Figure 3). Five of the fifteen compounds elicited a mix of non-competitive and competitive antagonist profiles at 5-HT_{3A} receptors (Figure 3). Tertiary tropane triazoles, TTTh-1, TTPh-18, and TToPy-1, showed the most potent competitive antagonist responses at a K_a of 100 nM or less with TTPh-18 showing the highest potency at a K_a of 54 nM (Table 1).

The α7 agonists generally showed a difference in potency between quaternary and tertiary tropane triazoles. Aside from the pair of *para*-positioned

pyridine which only showed a 10-fold difference, all other quaternary tropane triazole showed a 100-fold higher agonist potency for α7 than the tertiary tropane. The trend is reversed for the 5-HT_{3A} receptor where the tertiary competitive antagonists showed a 3 to 10-fold increase in antagonist potency compared to the quaternary competitive antagonists. This trend is not observed for the non-competitive antagonists.

The 1,2,3-triazole compounds had low potency at the α4β2 receptors with eight of the fourteen compounds displaying a K_a's of 25 μM or greater. QTmN-1 displayed the highest potency at 1.1 μM. No observable trend was discerned from the α4β2 data. (Table 1)

1,2,3-triazole compounds' binding affinity at α7 and 5-HT_{3A} intact cell receptors display similar trends to their functional characteristics

Intact cell receptor binding experiments were subsequently performed on α7, α4β2, and 5-HT_{3A} cells using radiolabeled [^{3}H] agonists ((±)-[^{3}H] epibatidine and (±)-[^{3}H] granisetron). Intact cells were incubated with radiolabeled [^{3}H] agonist along with competing triazole compounds over a course of 2 hours before being read in a scintillation counter for 16 hours. A Schild dose-response analysis was used to characterize the binding characteristics of each triazole compound using concentration-response curves with increasing triazole concentration.

For α7-nAChR, the compound rank order from the intact cell binding assays were similar to the responses in the Flex assay. The analysis showed quaternary compound QTIn-1 to be of the highest affinity at a K_d of 49 nM. The tertiary analogue of QTIn-1, TTIN-1, showed a K_d of 4.2 μM – a 100-fold decrease from the quaternary tropane (Figure 4). The quaternary compounds with the next highest affinity, QTTh-1, QTmN-1, QTPh-12, showed a 10-fold decrease in affinity, but still retained close to 100-fold difference compared to their tertiary analogues (Figure 4). This trend was also observed with the pyridines with lower affinity. Quaternary triazoles, QToPy-1, QTpPy-1, and QTmPy-1, each displayed a 10-fold or more increase in binding affinity compared to their tertiary analogues. (Table 2)

This trend was reversed for competitive antagonists at the 5-HT_{3A} intact cell receptors. Tertiary competitive antagonists, TTTh-1, TTPh-18, TToPy-1, and TTmPy-1, showed a K_d of around 1 μM while the *para*-positioned pyridine triazole, TTpPy-1, showed a low binding affinity at K_d of 18 μM (Table 2). The trend found for antagonism in the Flex functional assay holds true with the quaternary analogues displaying 2 to 4-fold decreased binding affinity compared to the tertiary analog (Figure 5). Overall, the tertiary tropanes at 5-HT_{3A} intact cell receptors had a higher affinity compared to α7 intact cell receptors, but there was a smaller difference in K_d between tertiary and quaternary tropanes at the 5-HT_{3A} receptors than at α7-nAChR.

Analysis of the triazole series of compounds at the α4β2 receptor did not show a K_d below 50 μM for any of the compounds and were not analyzed beyond the initial screening (Table 2).

The 1,2,3-triazole compounds at *Ls*, *Ac*, and *Ac* Y55W binding proteins exhibit similar binding characteristics as the α7 nAChR intact cells but diminished selectivity

The 1,2,3-triazole compounds were incubated with radiolabeled agonist, (±)-[^{3}H] epibatidine, at *Ls*, *Ac*, and *Ac*Y55W acetylcholine binding proteins. A Schild analysis was used to characterize binding activity through concentration-response curves. Since AChBPs are closer homologues to the α7 nAChRs than to α4β2 and 5-HT_{3A} receptors, quaternary tropane triazoles had higher affinity compared to their tertiary analogues across all three AChBPs. Comparing the K_d of the three proteins, the quaternary tropanes had an overall stronger binding affinity at *Ls* and *Ac* than at the *Ac*Y55W mutant, but the degree of difference is generally small, 2 to 4-fold. Tertiary tropanes displayed a greater variance among the three proteins than the quaternary tropanes, but the difference was obscured by their low binding affinity. Overall, similar to their selectivity at α7 receptors, quaternary tropanes had 2 to 10-fold higher binding affinity at the three binding protein interfaces than their respective tertiary analogues (Table 3). However this difference was smaller than at α7 nAChRs, revealing a distinction between AChBP and the nAChR subtypes. (Table 3)

The 1,2,3-triazoles at α7-similar *Aplysia californica* mutant, Ac α7 (1), show higher selectivity between tertiary and quaternary tropanes compared to wild-type *Ac*, and *Ac* Y55W

The 1,2,3-triazole compounds were incubated with α7-similar AchBP mutant, Ac α7 (1), to compete against radiolabeled (±)-[^{3}H] epibatidine. A Schild analysis was used to characterize binding activity through concentration-response curves. Overall, binding characteristics of triazole compounds on Ac α7 (1) displayed a higher affinity at the binding pocket for quaternary compounds than tertiary compounds. QTTh-1 and QTPh-12 displayed the highest affinity at a K_d of ~60 nM, which is 16 to 26-fold higher in binding affinity than their tertiary analogues (Table 4). In particular, the difference in selectivity between tertiary and quaternary compounds for the binding pocket was more apparent in Ac α7 (1) than wild-type *Ac* and *Ac* Y55W (Table 4). Even with lower affinity compounds, this trend holds true due to a decreased affinity for the tertiary tropanes at the binding pocket. Tertiary tropanes such as TTmN-1 and TTIn-1 displayed a binding affinity lower than 5 μM, a significant decrease compared to their activity at wild-type *Ac* and *Ac*Y55W (Table 4). This trend of Ac α7 (1)'s increased selectivity compares well with α7 receptor's selectivity, because the binding characteristics at the α7 receptor consistently show a 10-fold or greater difference in affinity between quaternary and tertiary tropanes. The only compounds that did not follow this trend were the *para*-positioned pyridines,

TTpPy-1 and QTpPy-1, both of which showed a similar micromolar binding affinity (Table 4).

The 1,2,3-triazole compounds at 5-HT$_{3A}$-similar *Ac* mutant, *Ac* 5-HT$_{3A}$ (1), proteins exhibit similar binding characteristics as the 5-HT$_{3A}$ intact cell receptors but do not mimic the overall trend

The 1,2,3-triazole compounds were incubated with 5-HT$_{3A}$-similar AChBP mutant, *Ac* 5-HT$_{3A}$ (1), to compete against radiolabeled (±)-[^{3}H] epibatidine. A Schild analysis was used to characterize binding activity through concentration-response curves. Analysis of binding characteristics showed similar binding affinities and a similar trend for the triazole compounds at *Ac* 5-HT$_{3A}$ (1) compared to *Ac* Y55W. In general, quaternary tropanes showed an increased binding affinity compared to their tertiary analogues, but the binding affinities of quaternary tropanes were decreased compared to wild-type *Ac*. Binding affinities of two tertiary compounds, TTTh-1 and TTIn-1, increased by 2 to 3-fold compared to their activity at *Ac* Y55w, and TTTh-1 in particular showed a K_d of 0.6 μM which is more similar to the binding affinity of the compound at the 5-HT$_{3A}$ receptor than at *Ac* or *Ac* Y55W. Interestingly, the majority of the pyridines elicited a significant loss in binding affinity to a K_d of higher than 5.0 μM. This change mirrors the lack of binding affinity of those compounds at the 5-HT$_{3A}$ receptor. Overall, the trend for binding activities of the triazole compounds at *Ac* 5-HT$_{3A}$ (1) mutant does not mimic those of the compounds at 5-HT$_{3A}$ intact cell

receptor, but we do see significant differences in binding characteristics of the triazoles at the mutant compared to the *Ac* and *Ac* Y55W. (Table 4)

The 1,2,3-triazole compounds at 5-HT_{3A}-similar *Ac* mutant, *Ac* 5-HT_{3A} (2), do not mimic the overall trend at 5-HT_{3A} intact cell receptor but show similarities in binding affinities

The 1,2,3-triazole compounds were incubated with 5HT_{3A}-similar AChBP mutant, *Ac* 5-HT_{3A} (2), to compete against radiolabeled (±)-[^{3}H] epibatidine. Schild analysis was used to characterize binding activity through concentration-response curves. In general, analysis of binding characteristics showed higher binding affinities for the compounds at *Ac* 5-HT_{3A} (2) compared to wild-type *Ac* and *Ac* Y55W. Tertiary tropanes, TTPh-18, TTpPy-1, TToPy-1, and TTmPy-1, showed higher binding affinities of K_d < 1 μM with *Ac* 5-HT_{3A} (2) compared to their low affinity (K_d > 5 μM) with *Ac* 5-HT_{3A} (1) (Table 4). In particular, the significant increases in affinity for TTPh-18 and TToPy-1 at the *Ac* 5-HT_{3A} (2) mutant resulted in binding affinities that are more similar to those of the compounds at 5-HT_{3A} intact cell receptors. Interestingly, *Ac* 5-HT_{3A} (2) is the only binding protein for which NTPh-2, the secondary tropane, displayed an affinity of 0.49 μM, making it remarkably similar to the compound's binding affinity at 5-HT_{3A} intact cell receptors of which the K_d is 0.51 μM (Table 4). Overall, the trend for binding activities of the triazole compounds at *Ac* 5-HT_{3A} (2) did not mimic the binding trend displayed by the compounds at 5-HT_{3A} intact cell receptor, but they

showed increased binding affinity for the tertiary tropanes than for quaternary tropanes, making it similar to the binding analysis at the 5-HT_{3A} intact cell receptor.

Table 1. Functional Activity of 1,2,3-Triazole Compounds at α7, α4β2, and 5-HT_{3A} Receptors

		Receptors (K_a, μM) (n ≥ 3)		
Name	**Structure**	**α7 (EC_{50})**	**α4β2**	**5-HT_{3A}**
TTTh-1	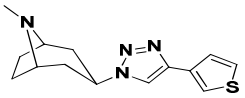	6.8 ± 1.9	25 + 15	0.1 + 0.02
QTTh-1	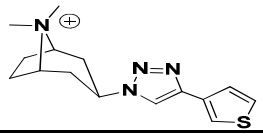	0.055 ± 0.024	26 ± 3.6	0.4 ± 0.2
TTmN-1	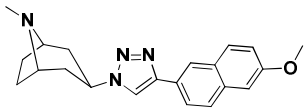	27.3 ± 13.35	2.0 ± 0.3	13 ± 4.0*
QTmN-1	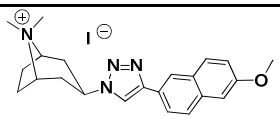	0.031 ± 0.0151	1.1 ± 0.6	15 ± 3.0*
TTPh-18	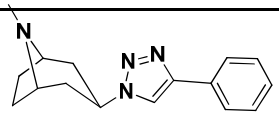	4.1 ± 1.18	6.5 ± 3.0	0.05 ± 0.02
QTPh-12	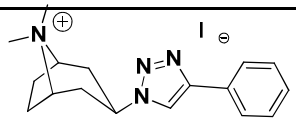	0.03 ± 0.010	4.5 ± 2.7	0.18 ± 0.11
NTPh-2	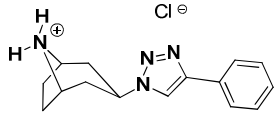	4.4 ± 2.05	6.5 ± 3.3	>30.0*
TTIn-1	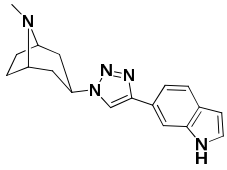	0.77 ± 0.305	2.7 ± 0.4	6.0 ± 3.7*
QTIn-1	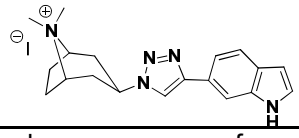	0.008 ± 0.0023	11 ± 6.4	1.6 ± 0.7*

Receptor functional assays were performed with the fluorescent Ca^{2+} CNiFER cell lines.
All α7 experiments were conducted in the presence of 10μM PNU-120596.
All values are reported with n = 3 or more experiments.
Compounds which did not pass the "quickscreens" are represented as > 30 μM
*Had mixed competitive and non-competitive inhibition.

Table 1. Functional Activity of 1,2,3-Triazole Compounds at α7, α4β2, and 5-HT_{3A} Receptors, Continued

		Receptors (K_a, μM) (n ≥ 3)		
Name	**Structure**	**α7 (EC_{50})**	**α4β2**	**5-HT_{3A}**
TToPy-1	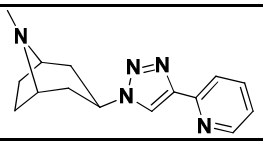	30 ± 11.6	>30.0	0.1 ± 0.03
QToPy-1	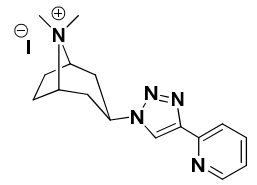	0.4 ± 0.3	>30.0	0.8 ± 0.3
TTpPy-1	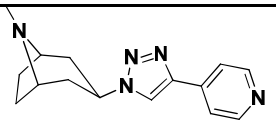	33 ± 12.0	>30.0	4.4 ± 1.4
QTpPy-1	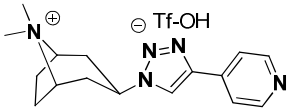	4.2 ± 1.83	>30.0	32 ± 19
TTmPy-1	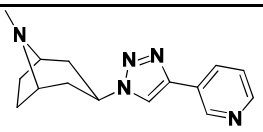	>30.0	>30.0	0.45 ± 0.05
QTmPy-1	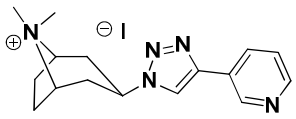	1.0 ± 0.8	>30.0	4.8 ± 0.5

Receptor functional assays were performed with the fluorescent Ca^{2+} CNiFER cell lines. All α7 experiments were conducted in the presence of 10μM PNU-120596.
All values are reported with n = 3 or more experiments.
Compounds which did not pass the "quickscreens" are represented as > 30 μM
*Had mixed competitive and non-competitive inhibition.

Table 2. Binding Characteristics of 1,2,3-Triazole Compounds at Intact Cell α7, α4β2, and 5-HT$_{3A}$ Receptors

		Receptors (K_i, μM) (n ≥ 3)		
Name	**Structure**	**α7**	**α4β2**	**5-HT$_{3A}$**
TTTh-1	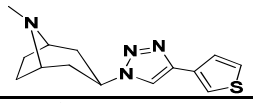	16 ± 2.0	>50	0.92 ± 0.21
QTTh-1	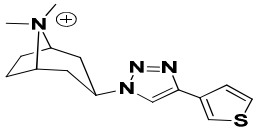	0.41 ± 0.16	>50	1.6 ± 0.28
TTmN-1	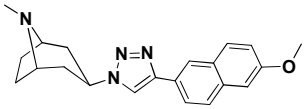	20 ± 9.0	>50	17 ± 6.6*
QTmN-1	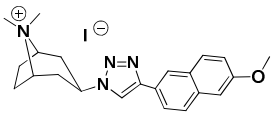	0.22 ± 0.091	>50	31 ± 8.6*
TTPh-18	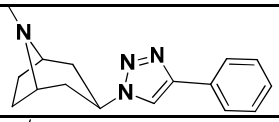	21 ± 9.6	>50	0.37 ± 0.015
QTPh-12	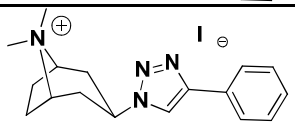	0.36 ± 0.026	>50	1.2 ± 0.089
NTPh-2	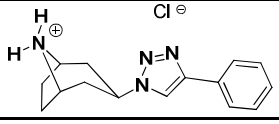	29 ± 9.8	>50	0.51 ± 0.067*
TTIn-1	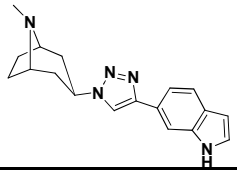	4.2 ± 2.8	>50	6.0 ± 0.78*
QTIn-1	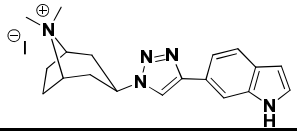	0.049 ± 0.0088	>50	4.9 ± 0.85*

Intact cell receptor binding assays were performed with the fluorescent Ca^{2+} CNiFER cell lines.
Binding values were calculated from SPA competition assay with [^{3}H]-epibatidine.
All α7 experiments were conducted using α7/5-HT$_{3A}$ chimaeric nAChRs.
All values are reported with n = 3 or more experiments.
Compounds which did not pass the "quickscreens" are represented as > 50 μM.
*Had mixed competitive and non-competitive inhibition.

Table 2. Binding Characteristics of 1,2,3-Triazole Compounds at Intact Cell α7, α4β2, and 5-HT$_{3A}$ Receptors, Continued

		Receptors (K_i, μM) (n ≥ 3)		
Name	**Structure**	**α7**	**α4β2**	**5-HT$_{3A}$**
TToPy-1	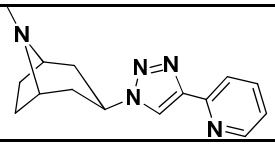	>50	>50	1.3 ± 0.10
QToPy-1	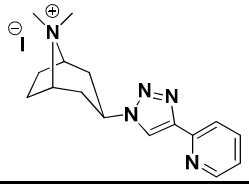	4.3 ± 2.0	>50	3.7 ± 1.1
TTpPy-1	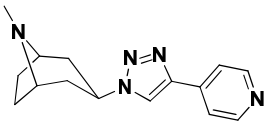	21 ± 16	>50	18 ± 12
QTpPy-1	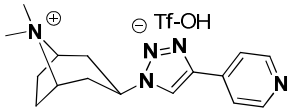	1.5 ± 0.45	>50	>50
TTmPy-1	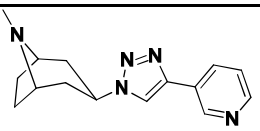	17 ± 3.0	>50	2.4 ± 0.84
QTmPy-1	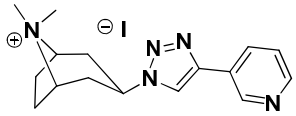	5.4 ± 0.72	>50	17 ± 8.1

Intact cell receptor binding assays were performed with the fluorescent Ca^{2+} CNiFER cell lines.
Binding values were calculated from SPA competition assay with [^{3}H]-epibatidine.
All α7 experiments were conducted using α7/5-HT$_{3A}$ chimaeric nAChR.
All values are reported with n = 3 or more experiments.
Compounds which did not pass the "quickscreens" are represented as > 50 μM.
*Had mixed competitive and non-competitive inhibition.

Table 3. Binding Characteristics of 1,2,3-Triazole Compounds at *Ls*, *Ac*, and *Ac* Y55W AChBPs

		AChBP (K_d, μM) (n ≥ 3)		
Name	**Structure**	***Ls***	***Ac***	***Ac* Y55W**
TTTh-1	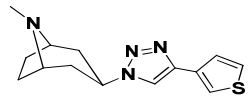	>5.0	>5.0	>5.0
QTTh-1	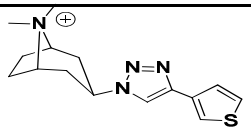	0.19 ± 0.028	0.073 ± 0.028	0.27 ± 0.083
TTmN-1	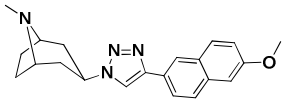	0.078 ± 0.011	0.12 ± 0.055	0.48 ± 0.066
QTmN-1	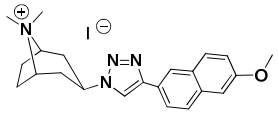	0.087 ± 0.0089	0.016 ± 0.012	0.038 ± 0.064
TTPh-18	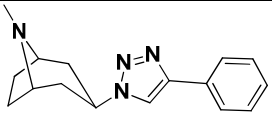	0.69 ± 0.005	0.67 ± 0.088	1.6 ± 0.24
QTPh-12	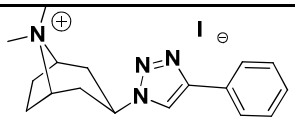	0.2 ± 0.025	0.15 ± 0.034	0.37 ± 0.036
NTPh-2	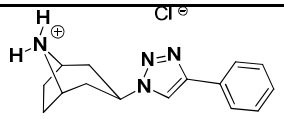	>5.0	>5.0	>5.0
TTIn-1	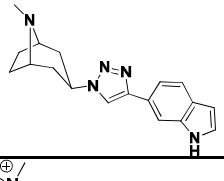	0.14 ± 0.084	0.32 ± 0.027	1.0 ± 0.056
QTIn-1	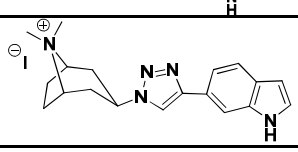	0.057 ± 0.017	0.35 ± 0.038	0.11 ± 0.011

AChBP binding values were calculated from SPA competition assay with [^{3}H]-epibatidine.
All values are reported with n = 3 or more experiments.
Compounds which did not pass the "quickscreens" are represented as > 5 μM.

Table 3. Binding Characteristics of 1,2,3-Triazole Compounds at *Ls*, *Ac*, and *Ac* Y55W AChBPs, Continued

		AChBP (K_d, μM) (n ≥ 3)		
Name	**Structure**	***Ls***	***Ac***	***Ac* Y55W**
TToPy-1	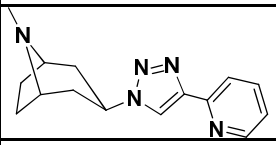	>5.0	1.2 ± 0.58	>5.0
QToPy-1	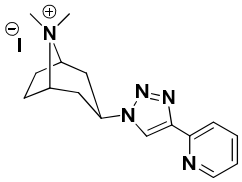	0.33 ± 0.24	0.22 ± 0.14	0.36 ± 0.1
TTpPy-1	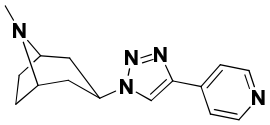	2.7 ± 0.68	0.72 ± 0.13	3.4 ± 0.3
QTpPy-1	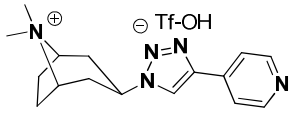	1.0 ± 0.2	0.39 ± 0.07	2.0 ± 0.32
TTmPy-1	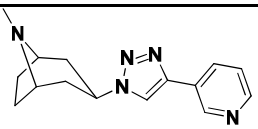	4.2 ± 0.074	1.1 ± 0.29	3.6 ± 0.74
QTmPy-1	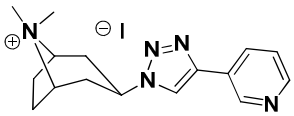	0.44 ± 0.36	0.15 ± 0.05	0.41 ± 0.34

AChBP binding values were calculated from SPA competition assay with [^{3}H]-epibatidine.
All values are reported with n = 3 or more experiments.
Compounds which did not pass the "quickscreens" are represented as > 5 μM.

Table 4. Binding Characteristics of 1,2,3-Triazole Compounds at *Ac* α7 (1), *Ac* 5-HT$_{3A}$ (1), and *Ac* 5-HT$_{3A}$ (2)

		AChBP (K_d, μM) (n ≥ 3)		
Name	**Structure**	***Ac* α7 (1)**	***Ac* 5-HT$_{3A}$ (1)**	***Ac* 5-HT$_{3A}$ (2)**
TTTh-1	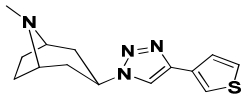	1.6 ± 0.51	0.60 ± 0.14	0.11 ± 0.009
QTTh-1	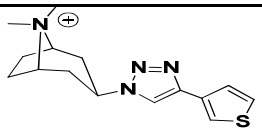	0.059 ± 0.015	0.23 ± 0.059	0.041 ± 0.014
TTmN-1	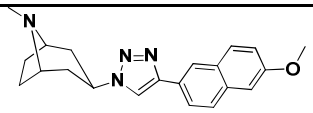	>5.0	0.72 ± 0.43	0.34 ± 0.16
QTmN-1	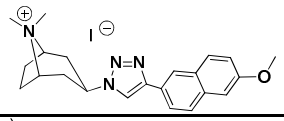	0.68 ± 0.07	0.047 ± 0.0097	0.034 ± 0.013
TTPh-18	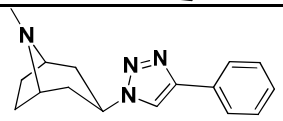	1.1 ± 0.027	>5.0	0.13 ± 0.016
QTPh-12	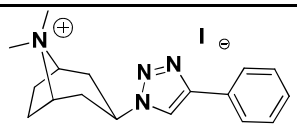	0.065 ± 0.006	0.22 ± 0.077	0.16 ± 0.055
NTPh-2	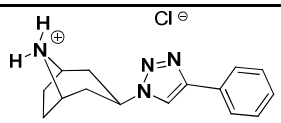	>5.0	>5.0	0.49 ± 0.17
TTIn-1	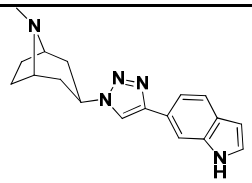	>5.0	0.52 ± 0.32	0.23 ± 0.073
QTIn-1	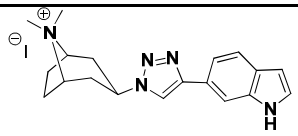	0.28 ± 0.028	0.097 ± 0.02	0.023 ± 0.009

AChBP binding values were calculated from SPA competition assay with [^{3}H]-epibatidine.
All values are reported with n = 3 or more experiments.
Compounds with values which did not pass the "quickscreens" are represented as > 5 μM.

Table 4. Binding Characteristics of 1,2,3-Triazole Compounds at *Ac* α7 (1), *Ac* 5-HT$_{3A}$ (1), and *Ac* 5-HT$_{3A}$ (2), Continued

		AChBP (K_d, μM) (n ≥ 3)		
Name	**Structure**	***Ac* α7 (1)**	***Ac* 5-HT$_{3A}$ (1)**	***Ac* 5-HT$_{3A}$ (2)**
TToPy-1	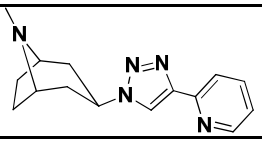	>5.0	>5.0	0.45 ± 0.091
QToPy-1	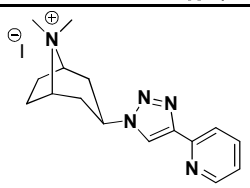	0.22 ± 0.063	0.380 ± 0.11	0.13 ± 0.021
TTpPy-1	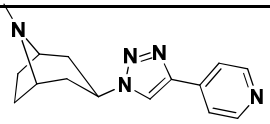	2.4 ± 1.48	>5.0	0.27 ± 0.10
QTpPy-1	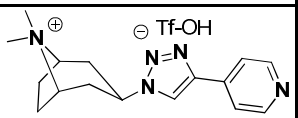	2.6 ± 0.29	>5.0	0.19 ± 0.045
TTmPy-1	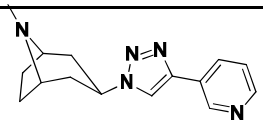	>5.0	>5.0	0.29 ± 0.089
QTmPy-1	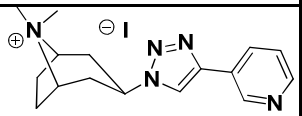	1.5 ± 0.61	0.61 ± 0.22	0.11 ± 0.032

AChBP binding values were calculated from SPA competition assay with [^{3}H]-epibatidine.
All values are reported with n = 3 or more experiments.
Compounds with values which did not pass the "quickscreens" are represented as > 5 μM.

Table 5. Protein Identity and Sequence Similarity of LGICs and AChBPs

Receptor : AChBP	Identity (%)	Similarity (%)
hα7-nAChR : *Ac*	28.7	60.9
hα4-nAChR : *Ac*	29.1	60.1
hβ2-nAChR : *Ac*	25.1	56.4
m5-HT_{3A} : *Ac*	24.9	54.8
hα7-nAChR : *Ls*	27.3	58.5
hα4-nAChR : *Ls*	25.3	56.6
hβ2-nAChR : *Ls*	23.1	53.8
m5-HT_{3A} : *Ls*	22.6	56.7
hα7-nAChR : *Ac*-MT1[a]	33.2	63.8
hα7-nAChR : *Ac*-MT2[a]	36.2	64.3
hα7-nAChR : *Ac*-MT3[ab]	39.7	66.8

[a]Mutants of *Ac* AChBP are denoted as *Ac*-MT1, 2, or 3 reported in (Nemecz and Taylor, 2011).
[b]Ac α7 (1) is used to denote *Ac*-MT3 for this thesis.

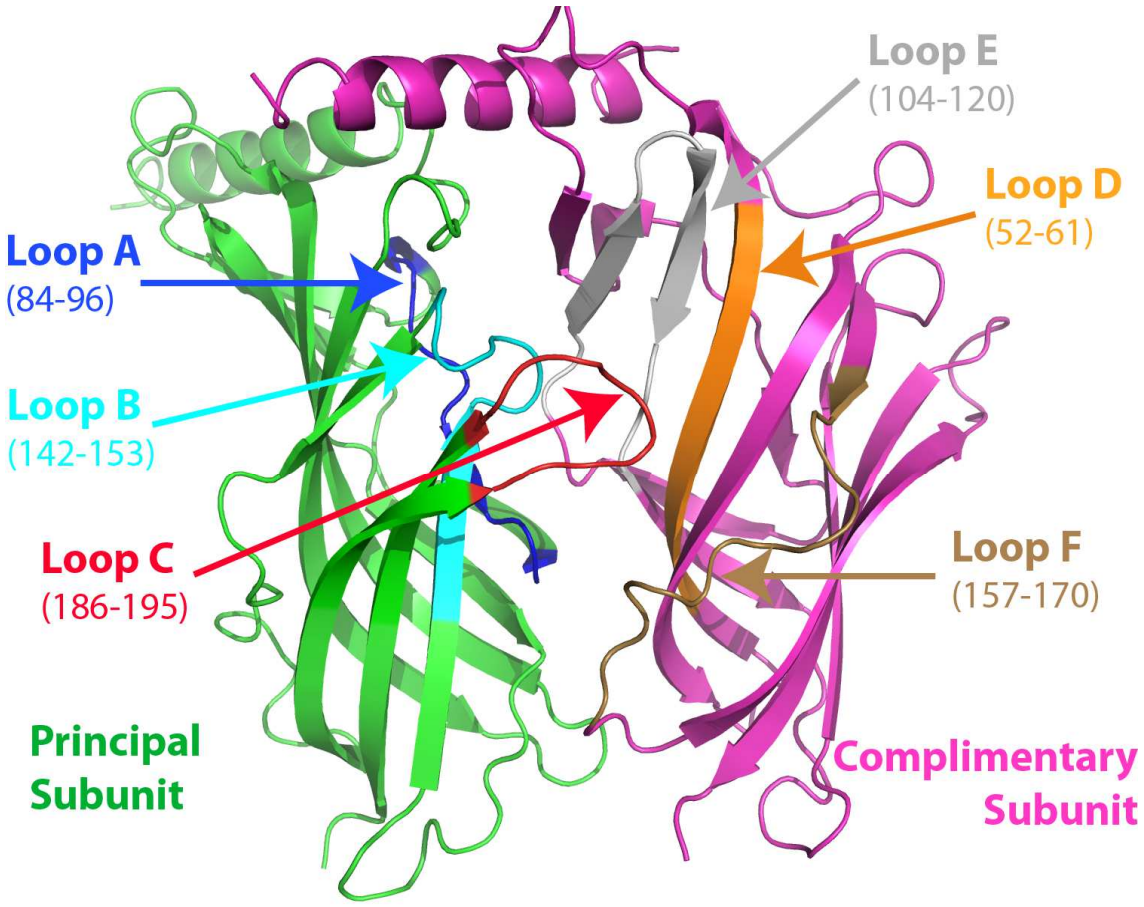

Figure 1. Loop regions of subunit interface for AChBP binding site
Two *Aplysia californica* subunits show the ligand binding interface. Loops A, B, and C represent the principal subunit (colored green) while Loops E, D, and F represent the complementary subunit (colored magenta). Figure generated using Pymol. Structure taken from PDB: 2BYQ, Ac-AChBP in complex with epibatidine (Hansen et al., 2005).

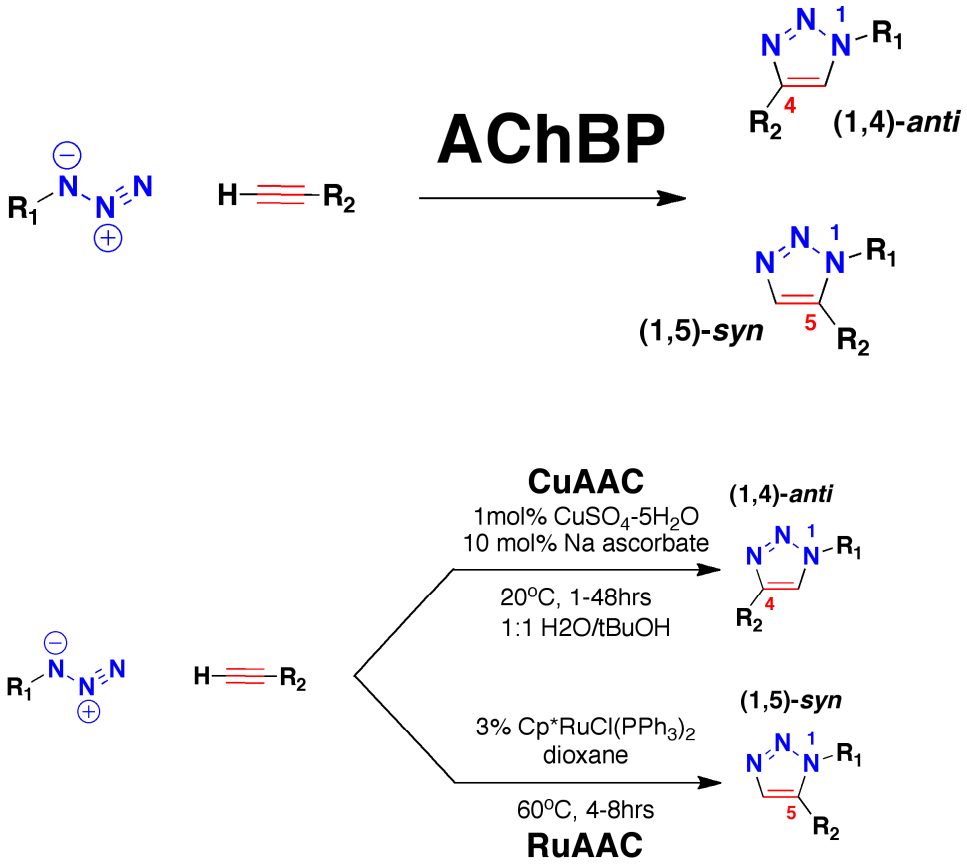

Figure 2. Schemes of *in situ* cycloaddition reaction of triazole
The cycloaddition of azide and alkyne building blocks at AChBP binding interfaces form products in either (1,4)-*anti* or (1,5)-*syn* isomer conformations. The building blocks that formed the triazoles are then identified, and they are synthesized in large amounts using Cu(I)-catalyzed azide-alkyne cycloaddition (CuAAC) to generate (1,4)-*anti*-regioisomers. (Yamauchi et al., 2012)

A.

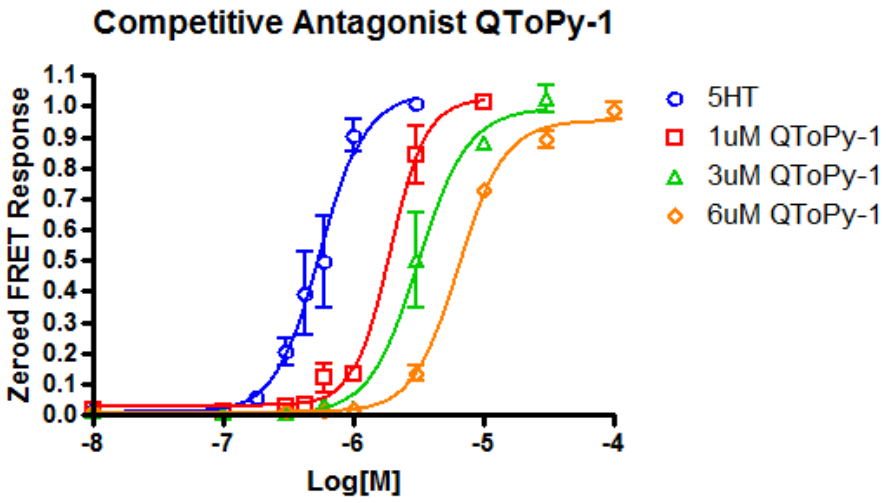

B.

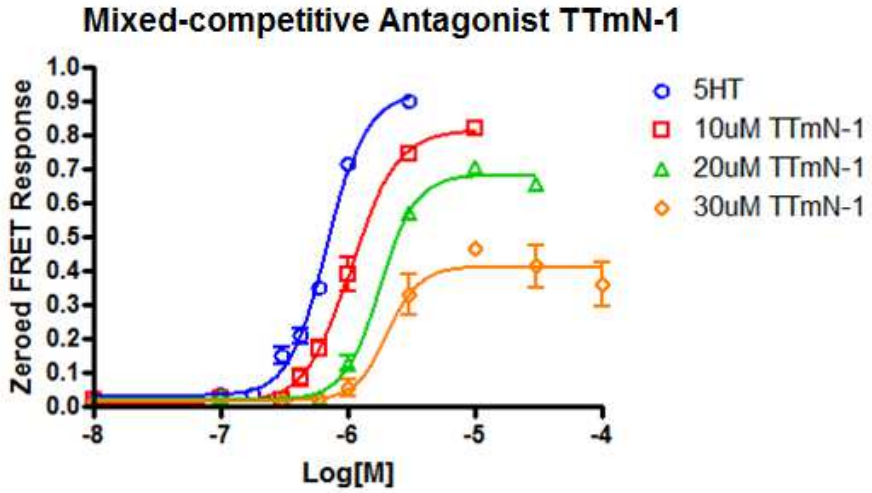

Figure 3. Competitive and mixed-competitive antagonism

A. Competitive antagonism of 5-HT elicited response on 5-HT_{3A} CNiFER cell by QToPy-1. The EC_{50} values for each curve shifted from 560 nM to 1.9 μM, 3.1 μM, and 6.3 μM for 1 μM, 3 μM, 6 μM QToPy-1 respectively.

B. Mixed-competitive antagonism of 5-HT elicited response on 5-HT_{3A} CNiFER cell by TTmN-1. The EC_{50} values for each curve shifted from 650 nM to 2.1 μM, 4.5 μM, and 4.8 μM for 10 μM, 20 μM, 30 μM TTmM-1 respectively, showing competitive inhibition. The maximum response decreases from 0.92 to 0.86, 0.67, and 0.41 for 10 μM, 20 μM, 30 μM TTmM-1 respectively, showing non-competitive inhibition.

A.

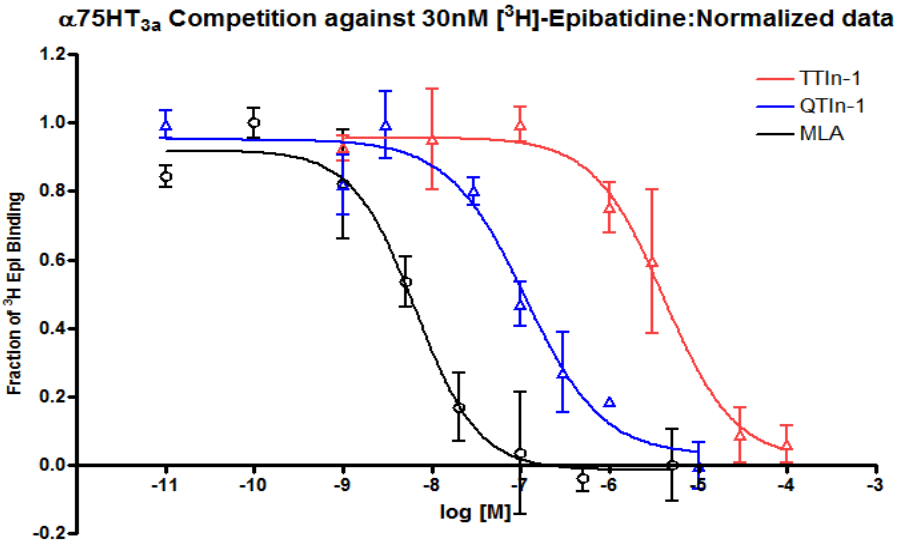

B.

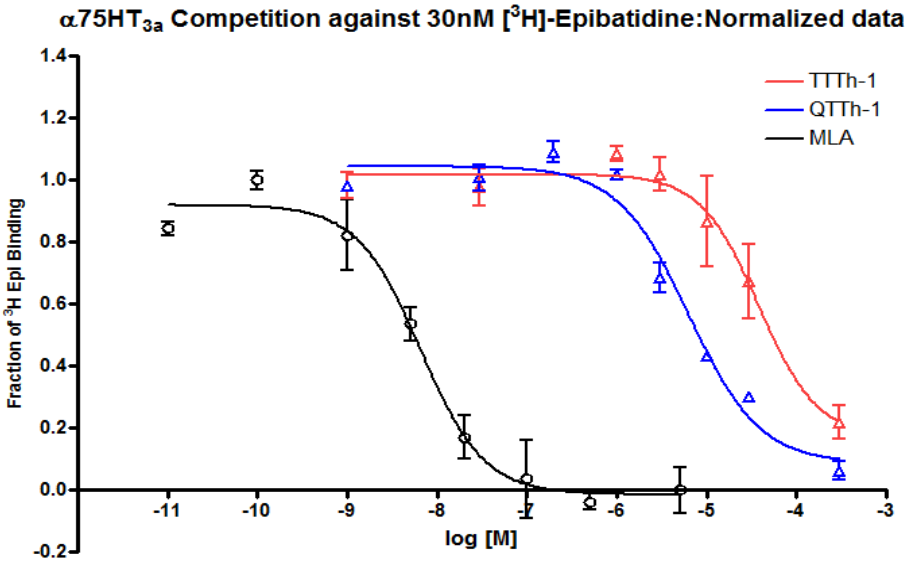

Figure 4. Comparison of binding characteristics between quaternary and tertiary tropane triazoles at α7 nAChR

A. In competitive binding against 30nM [^{3}H]-epibatidine, quaternary QTIn-1 produced a K_d of 0.045 μM, while tertiary TTIn-1 produced a K_d of 1.6 μM. MLA was used as the antagonist control.

B. In competitive binding against 30nM [^{3}H]-epibatidine, quaternary QTTh-1 produced a K_d of 2.5 μM, while tertiary TTTh-1 produced a K_d of 15 μM. MLA was used as the antagonist control.

C.

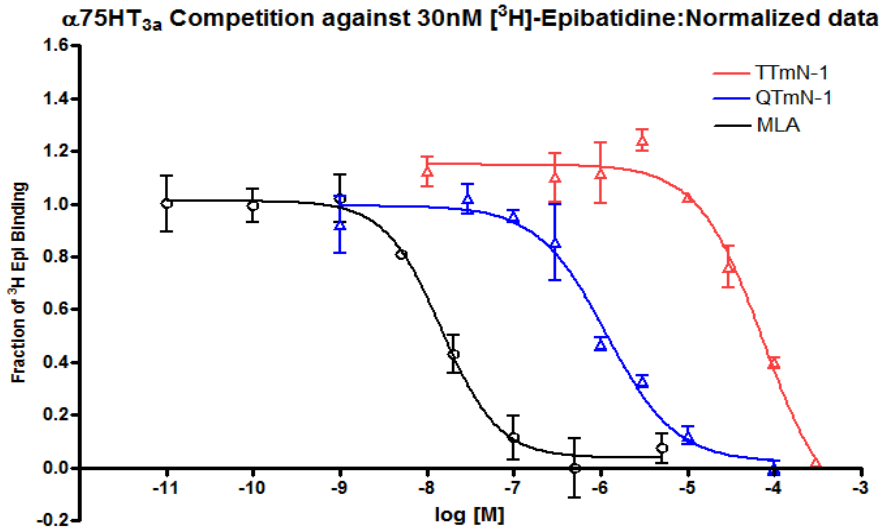

D.

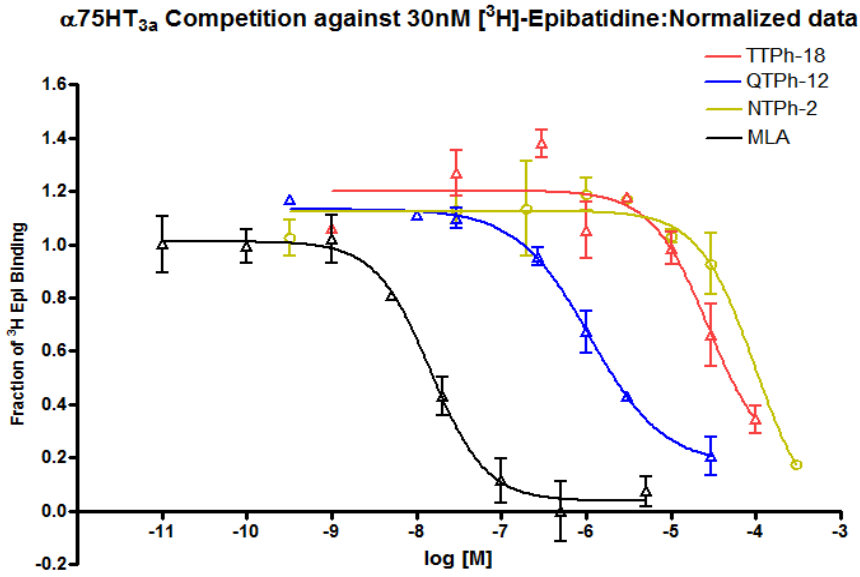

Figure 4. Comparison of binding characteristics between quaternary and tertiary tropane triazoles at α7 nAChR , continued

C. In competitive binding against 30nM [^{3}H]-epibatidine, quaternary QTmN-1 produced a K_d of 0.47 μM, while tertiary TTmN-1 produced a K_d of 30 μM. MLA was used as the antagonist control.

D. In competitive binding against 30nM [^{3}H]-epibatidine, quaternary QTPh-12 produced a K_d of 0.44 μM, while tertiary TTPh-18 produced a K_d of 11 μM. Secondary NTP-2 had a K_d of 40 μM. MLA was used as the antagonist control.

A.

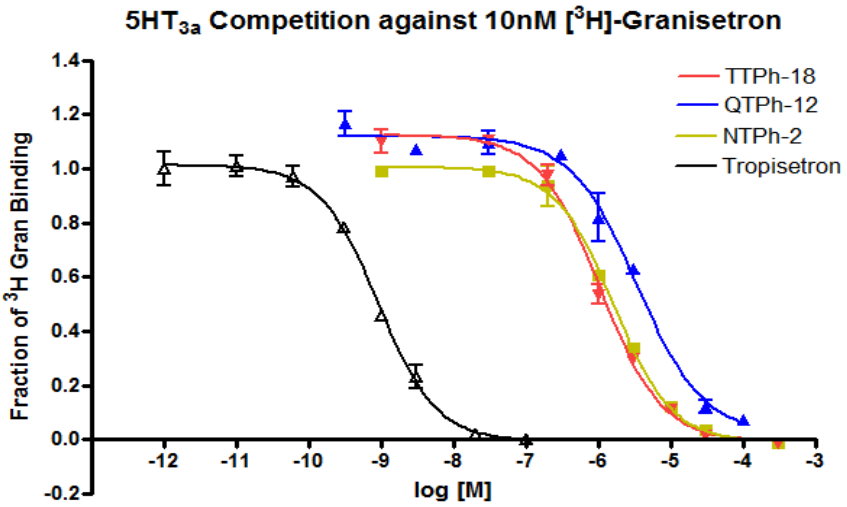

B.

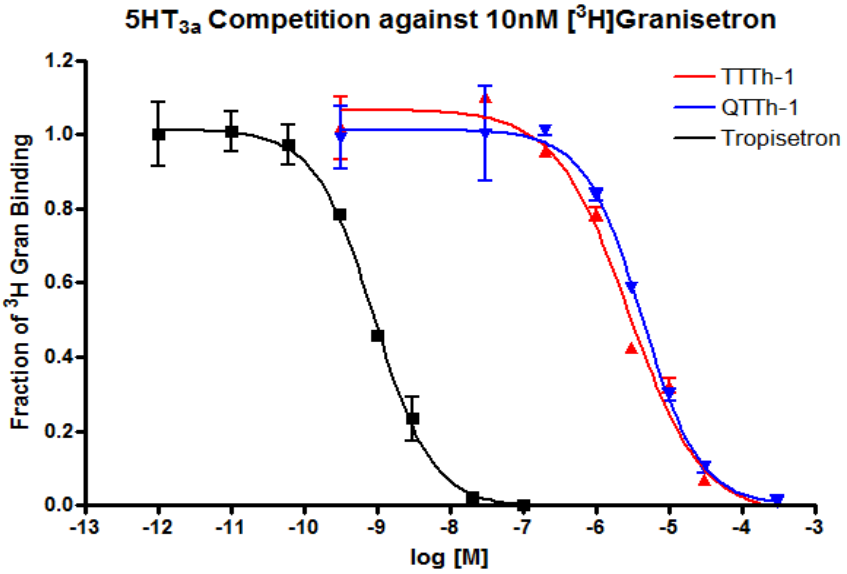

Figure 5. Comparison of binding characteristics between quaternary and tertiary tropane triazoles at 5-HT$_{3A}$ receptor

A. In competitive binding against 10nM [^{3}H]-granisetron, quaternary QTPh-12 produced a K_d of 1.1 μM, while tertiary TTPh-1 produced a K_d of 0.35 μM. Seconday NTPh-2Tropisetron showed a K_d of 0.54 μM. Tropisetron was used as the antagonist control.

B. In competitive binding against 10nM [^{3}H]-granisetron, quaternary QTTh-12 produced a K_d of 1.4 μM, while tertiary TTTh-1 produced a K_d of 0.92 μM. Tropisetron was used as the antagonist control.

C.

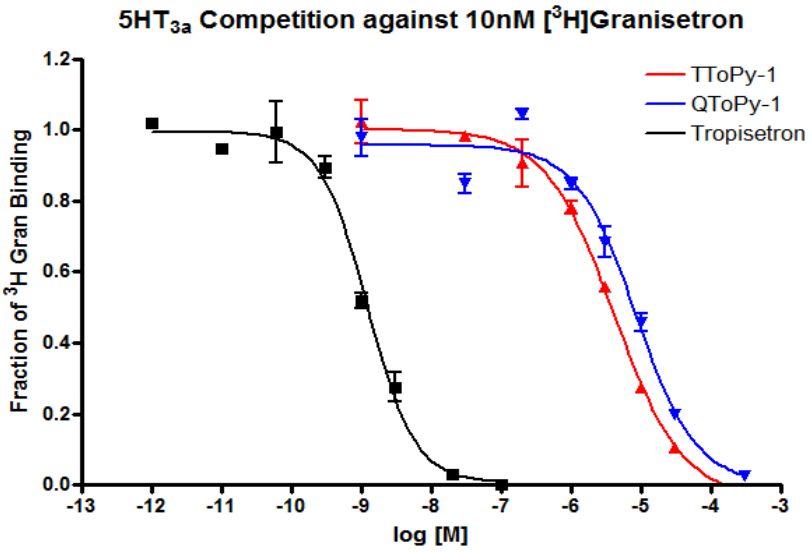

D.

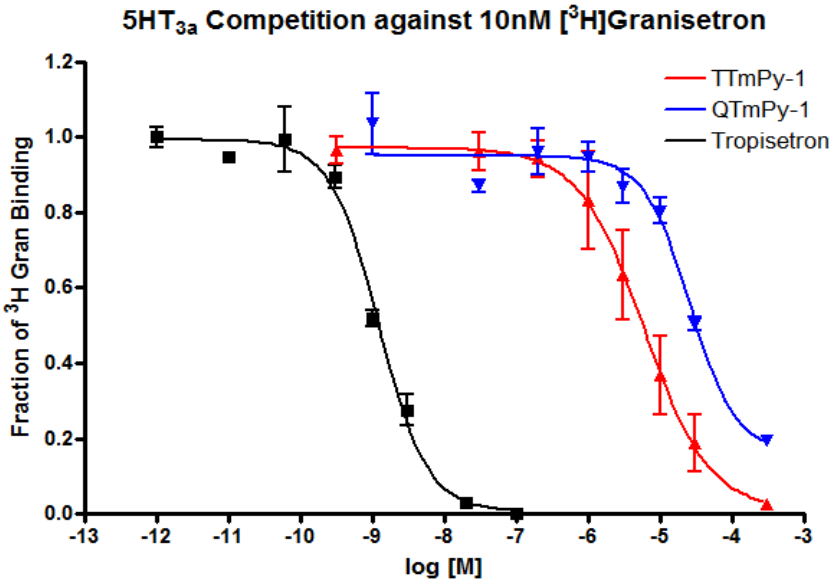

Figure 5. Comparison of binding characteristics between quaternary and tertiary tropane triazoles at 5-HT$_{3A}$ receptor, continued

C. In competitive binding against 10nM [^{3}H]-granisetron, quaternary QToPy-1 produced a K_d of 2.8 μM, while tertiary TToPy-1 produced a K_d of 0.1.3 μM. Tropisetron was used as the antagonist control.

D. In competitive binding against 10nM [^{3}H]-granisetron, quaternary QTmPy-1 produced a K_d of 8.5 μM, while tertiary TTmPy-1 produced a K_d of 2.0 μM. Tropisetron was used as the antagonist control.

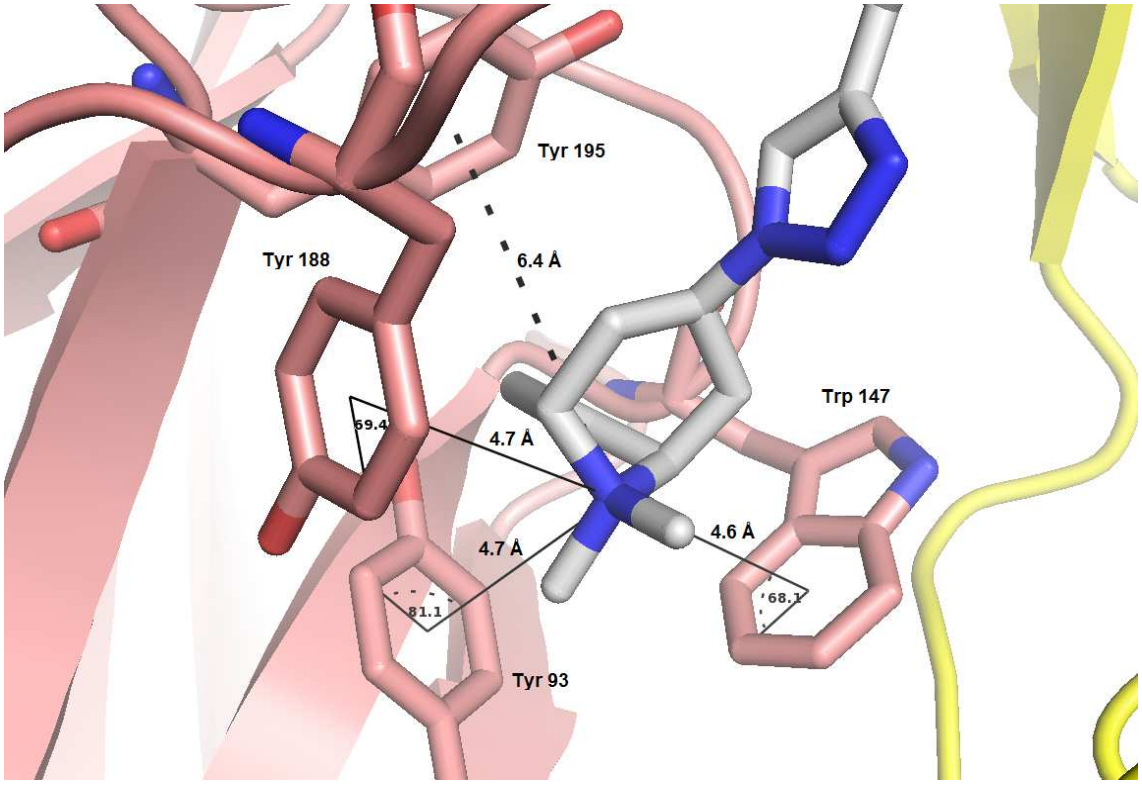

Figure 6. Crystal structure data of quaternary tropane, QTPh-12, in the aromatic nest of *Ac* AChBP

Triazole, QTPh-12, in complex with *Ac* AChBP show triazole's tropane ring and nitrogen facing towards the principal subunit and interacting with three aromatic residues (Tyr 93, Trp 147, and Tyr 188) at optimal cation-π range (4.5-5.5 Å) and at optimal angle (10-30° from the normal of the center of the rings). Distance of Tyr 195 is measured at 6.4 Å, showing that it is out of optimal cation-π range for the quaternary tropane.

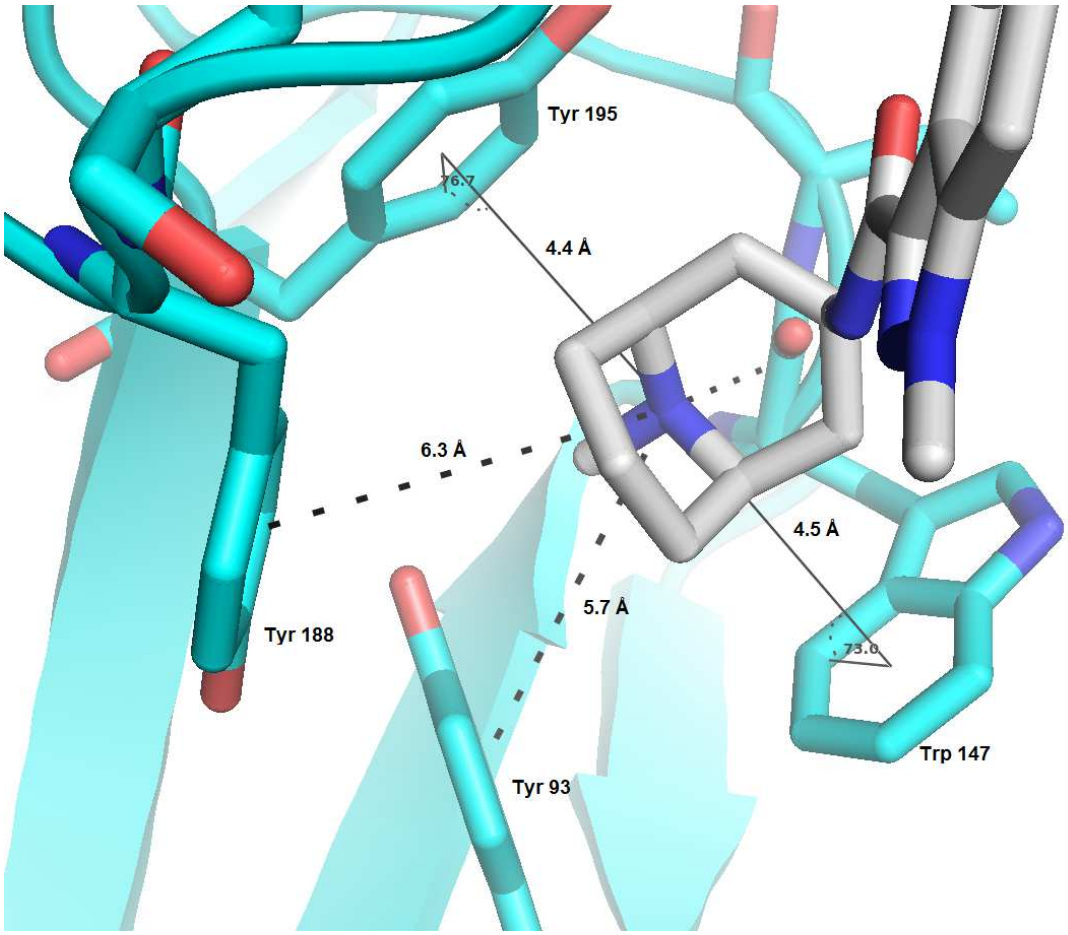

Figure 7. Crystal structure data of tertiary tropane, granisetron, in the aromatic nest of *Ac* AChBP

5-HT$_{3A}$ receptor antagonist granisetron in complex with *Ac* AChBP show compound's tropane ring and nitrogen facing towards the principal subunit and interacting with two aromatic residues (Trp 147, and Tyr 195) at optimal cation-π range (4.5-5.5 Å) and at optimal angle (10-30° from the normal of the center of the rings). Distance of Tyr 93 and Tyr 188 are measured at 5.7 Å and 6.4 Å respectively, showing that they are out of optimal cation-π range for the tertiary tropane. PDB ID: 2YME.

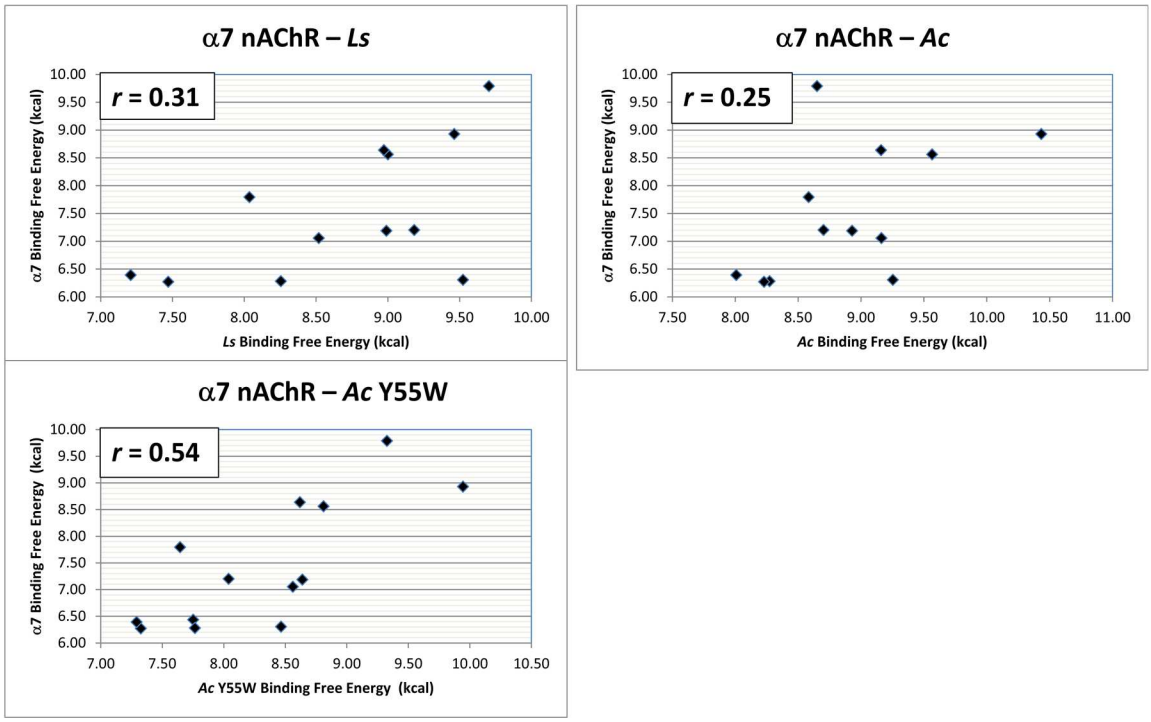

Figure 8.1. Correlation of α7 nAChR intact cell receptor binding free energy with *Ls*, *Ac*, and *Ac* Y55W binding free energy

Conversion to Gibbs free energy was used to correlate the binding values of triazole compounds at α7 nAChR and AChBPs. K_d values were converted to free energy using the equation $\Delta G^\circ = -RT \ln K_d$ where R is the gas constant 1.98 cal/degree*mole and T is the absolute temperature (Taylor and Insel, 1990). Correlation was done using Microsoft Excel to obtain a Pearson correlation coefficient (r).

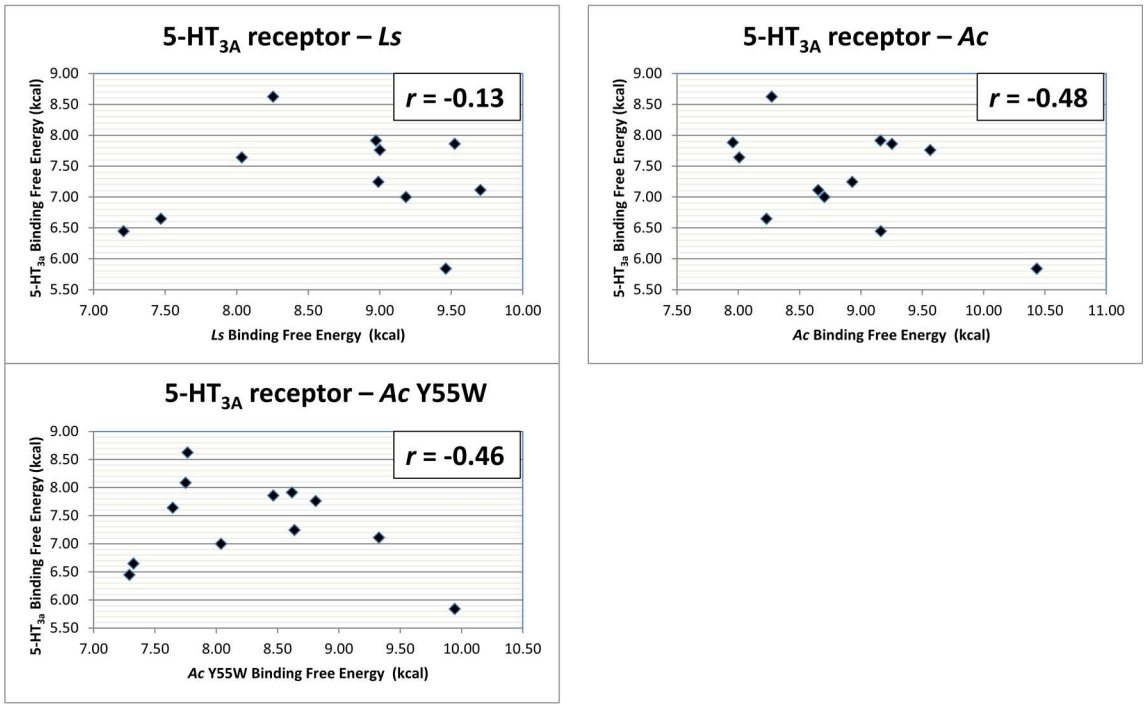

Figure 8.2. Correlation of 5-HT$_{3A}$ intact cell receptor binding free energy with *Ls*, *Ac*, and *Ac* Y55W binding free energy

Conversion to Gibbs free energy was used to correlate the binding values of triazole compounds at 5-HT$_{3A}$ receptor and AChBPs. K_d values were converted to free energy using the equation $\Delta G^{\circ} = -RT \ln K_d$ where R is the gas constant 1.98 cal/degree*mole and T is the absolute temperature (Taylor and Insel, 1990). Correlation was done using Microsoft Excel to obtain a Pearson correlation coefficient (r).

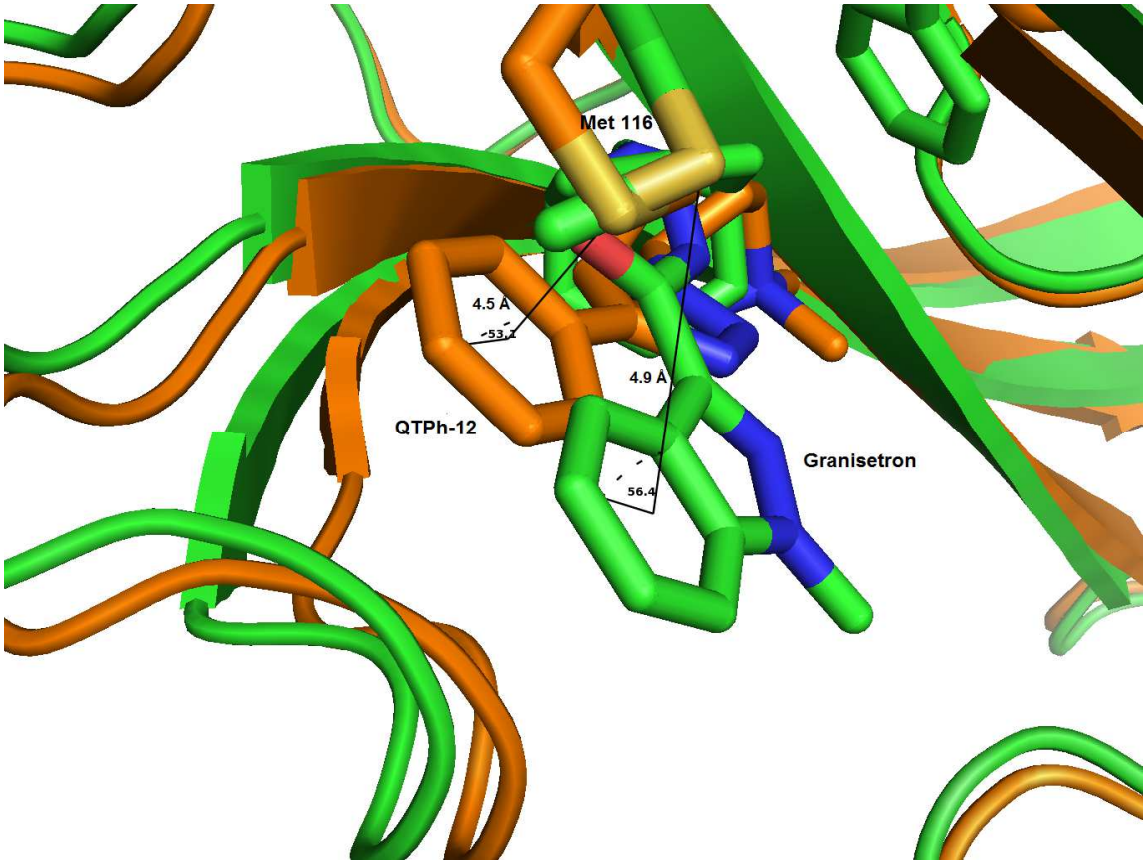

Figure 9.1. Crystal structure data shows Met 116 interaction with tropane compounds in *Ac* AChBP

Both quaternary tropane, QTPh-12, in complex with Ac (orange) and tertiary tropane, granisetron, in complex with *Ac* 5-HT$_{3A}$ (1) (green) are shown at distance (4.5 Å and 4.9 Å) and angle (~40°) from Met 116 residue, appropriate for strong sulfur-aromatic interaction. PDB ID: 2YME (*Ac* 5-HT$_{3A}$ (2)-gran).

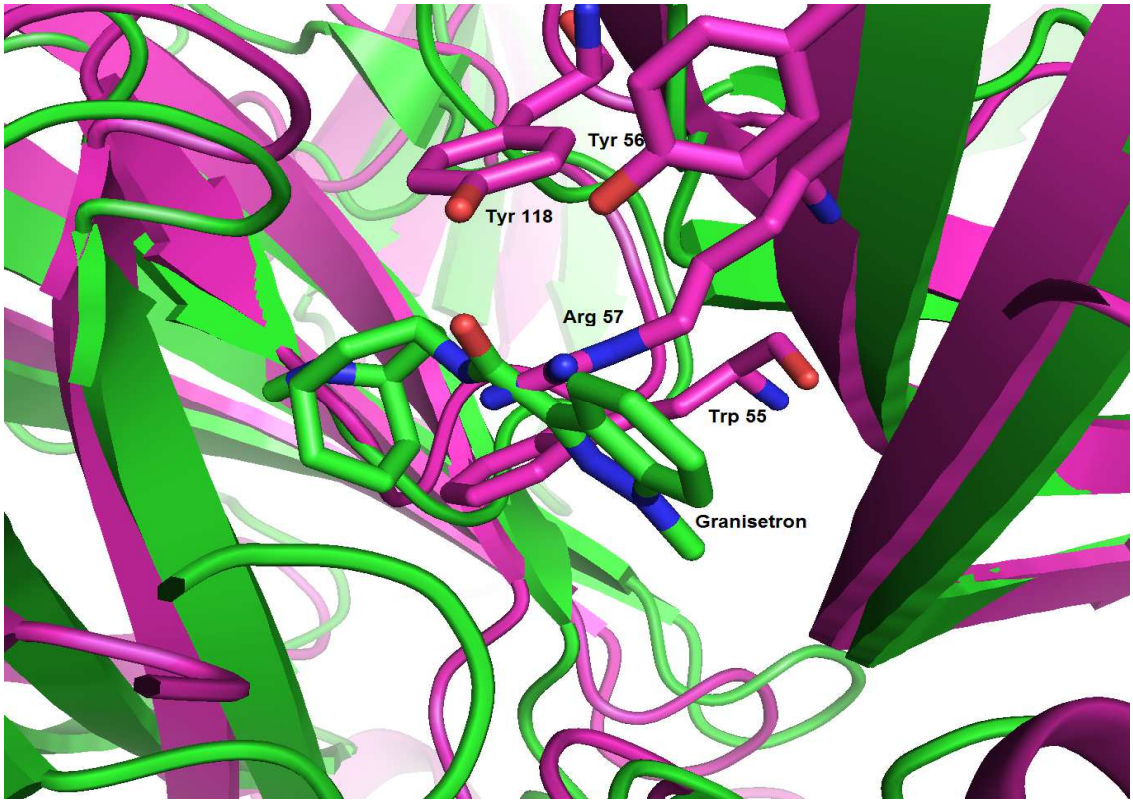

Figure 9.2. Crystal structure data of m5-HT$_{3A}$ receptor reveals possible interaction of Trp 55, Tyr 56, Arg 57, and Tyr 118 residues with granisetron
Mouse 5-HT$_{3A}$ receptor crystal (colored magenta) is overlaid onto granisetron in complex with *Ac* 5-HT$_{3A}$ (2) (colored green). 4 residues in the complementary subunit show possible interactions with granisetron. Tyr 118 from Loop E and Tyr 56 from Loop D show possible hydrogen bonding complex with the carbonyl linker of the granisetron, while Trp 55 and Arg 57 on Loop D could interact through cation-π with the tropane or indazole. PDB IDs: 4PIR (m5-HT$_{3A}$) and 2YME (*Ac* 5-HT$_{3A}$ (2)-gran).

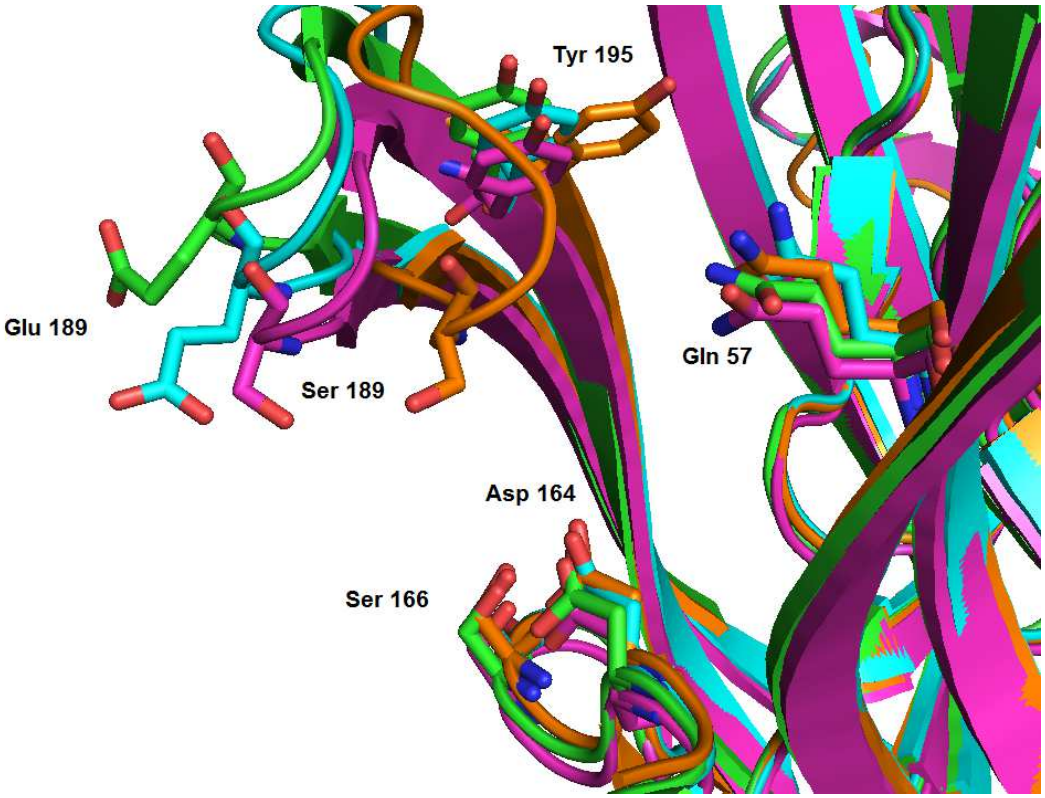

Figure 10. Subunit overlays of *Ac* WT and *Ac* α7 (1) AChBPs
Overlay of *Ac* WT in complex with QTTh-1 (agonist, colored orange), *Ac* WT-Apo (no ligand, colored magenta), *Ac* α7 (1)-Apo (no ligand, colored cyan), and *Ac* α7 (1) in complex with MLA (antagonist, colored green). Residues on Loop D and Loop F show similar poses throughout the overlay, while residues on Loop C, due to mutations in the linker, show a shift. Residue Glu 189 (mutated from Ser 189 in *Ac* α7 (1)) show a general shift away from binding pocket compared to Ser 189, and this shift is also shown in Tyr 195 in its distance from the pocket. Ser 189 of Ac WT with QTTh-1 show possible hydrogen bonding complexes with Loops D and F. PDB IDs: 2BYN (Ac WT-Apo), 3T4M (*Ac* α7 (1)-Apo), and 3SH1 (*Ac* α7 (1)-MLA).

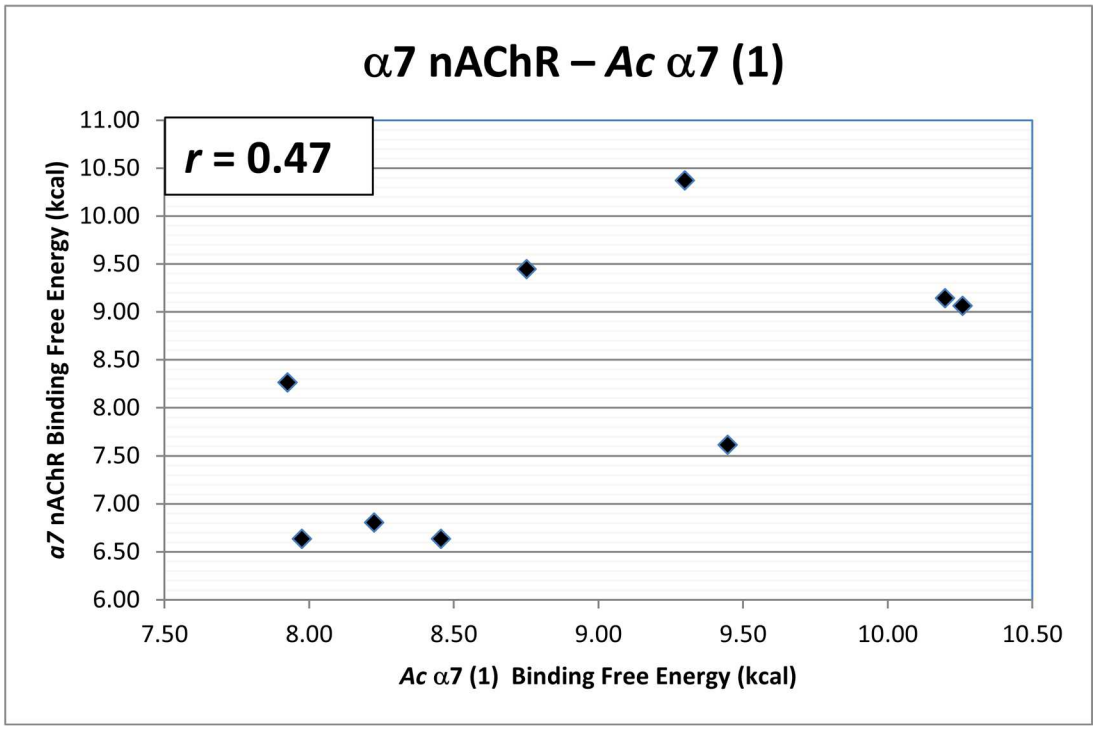

Figure 11. Correlation of α7 nAChR intact cell receptor binding free energy with *Ac* α7 (1) binding free energy

Conversion to Gibbs free energy was used to correlate the binding values of triazole compounds at α7 nAChR and *Ac* α7 (1). K_d values were converted to free energy using the equation $\Delta G^{\circ} = -RT \ln K_d$ where *R* is the gas constant 1.98 cal/degree*mole and *T* is the absolute temperature (Taylor and Insel, 1990). Correlation was done using Microsoft Excel to obtain a Pearson correlation coefficient (*r*).

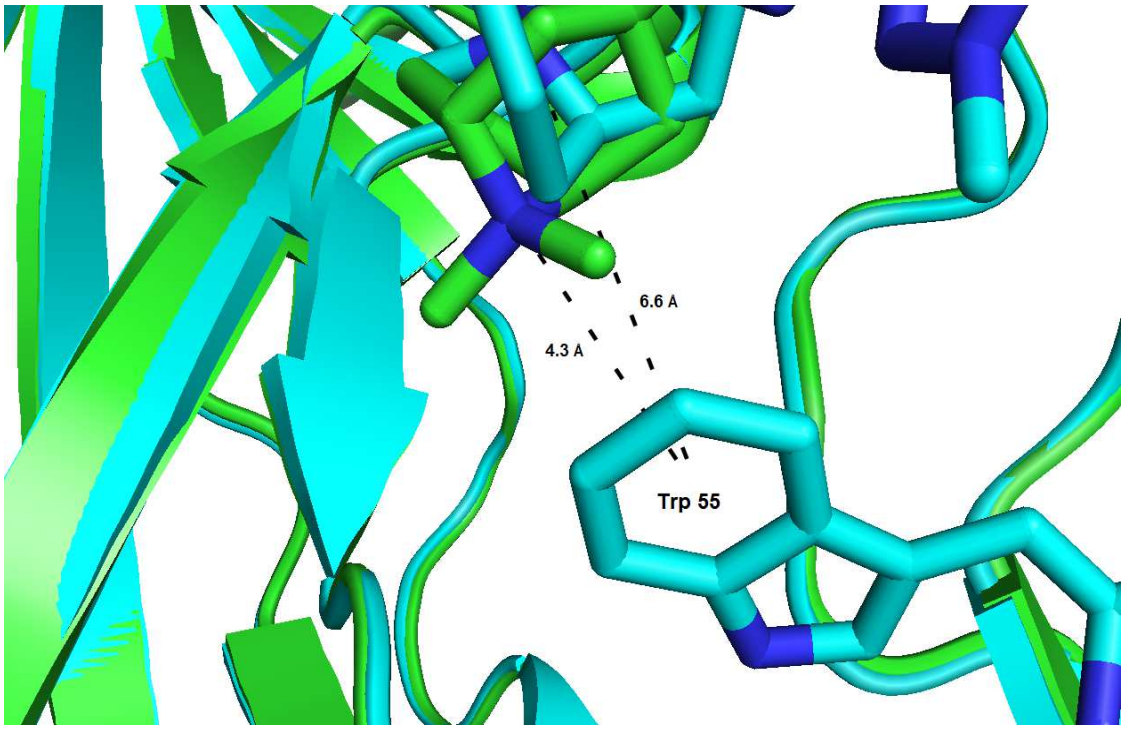

Figure 12. Crystal structure shows quaternary and tertiary tropane interaction with Trp 55

Quaternary tropane of QTIn-1 in *Ac* (colored green) show ~2.3 Å distance closer to Trp 55 than Tertiary tropane of granisetron (colored cyan). 4.3 Å from center of the Trp ring to quaternary nitrogen allows for strong cation-π interaction. PDB ID: 2YME.

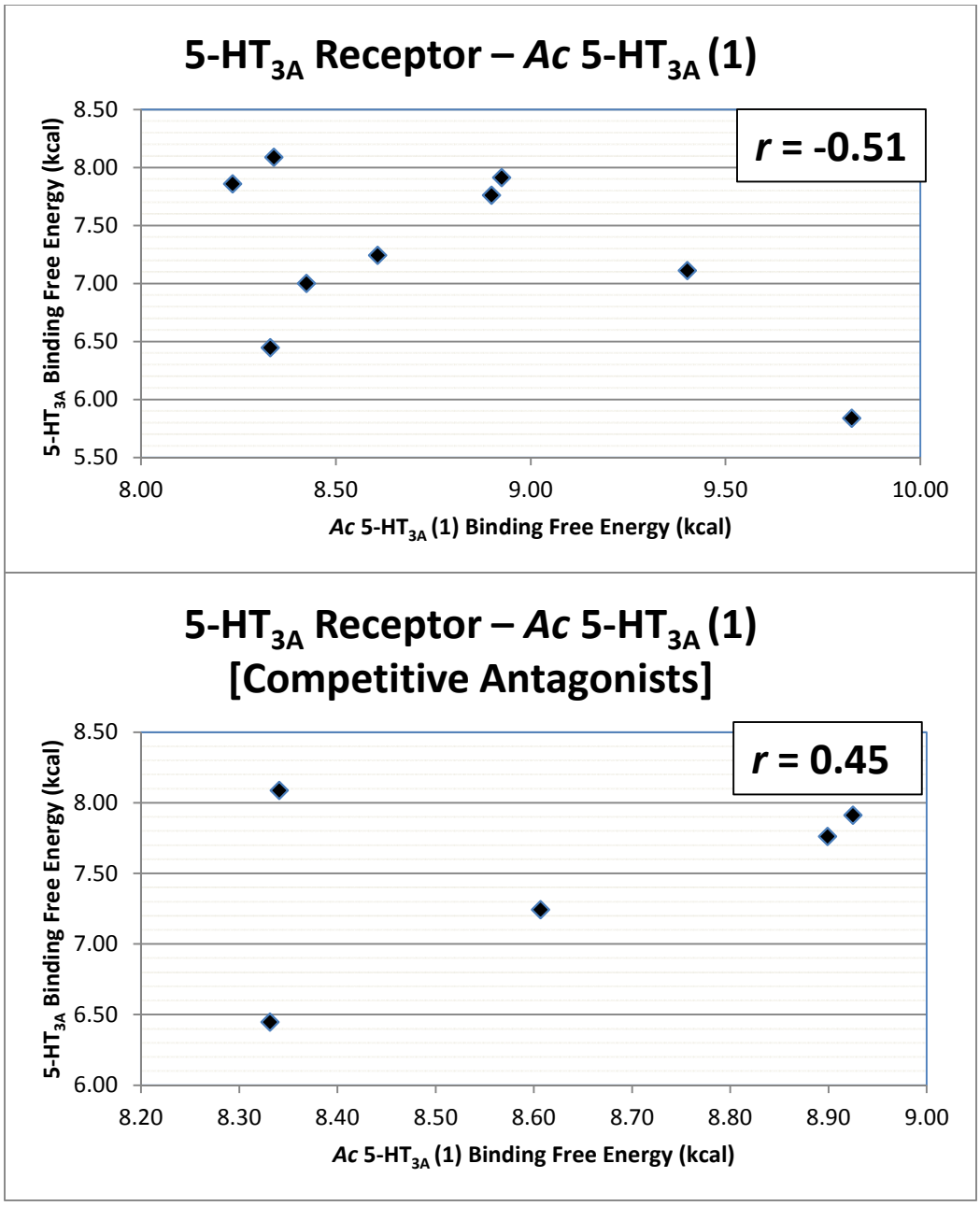

Figure 13. Correlation of 5-HT$_{3A}$ intact cell receptor binding free energy with *Ac* 5-HT$_{3A}$ (1) binding free energy

Conversion to Gibbs free energy was used to correlate the binding values of triazole compounds at 5-HT$_{3A}$ receptor and *Ac* 5-HT$_{3A}$ (1). K_d values were converted to free energy using the equation $\Delta G^{\circ} = -RT \ln K_d$ where R is the gas constant 1.98 cal/degree*mole and T is the absolute temperature (Taylor and Insel, 1990). Correlation was done using Microsoft Excel to obtain a Pearson correlation coefficient (r).

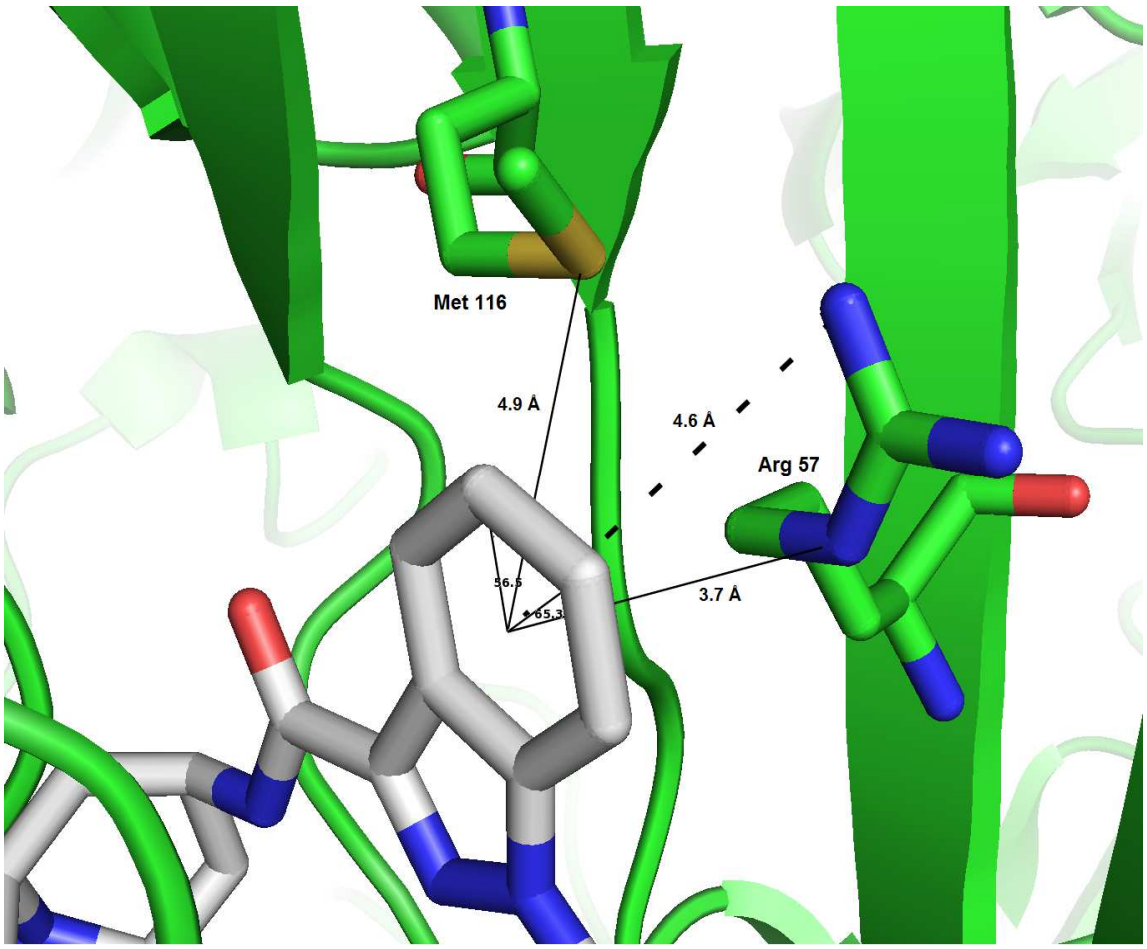

Figure 14.1. Crystal structure shows *Ac* 5-HT$_{3A}$ (2) granisetron interactions Arg 57 & Met 116

Granisetron in complex with *Ac* 5-HT$_{3A}$ (2) shows close distances to both Arg 57 (mutated from Gln 57 in *Ac* 5-HT$_{3A}$ (2)) and Met 116 (conserved). The indazole center is 3.7 Å and 4.6 Å from the two closest nitrogens of Arg 57, signifying strong cation-π interaction. Distance from center to Met 116 remains in range of sulfur-aromatic interaction and may affect granisetron interaction in the pocket. PDB ID: 2YME.

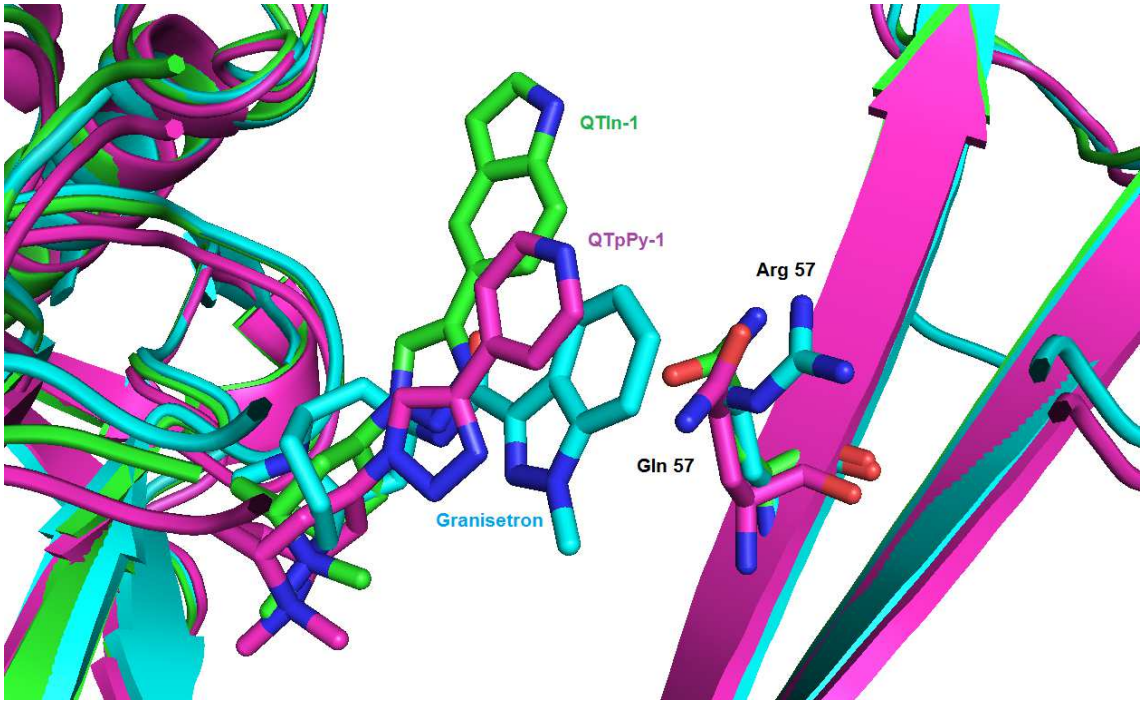

Figure 14.2. Crystal structure data show the different orientations of QTpPy-1, QTIn-1, and granisetron in the binding pocket

QTpPy-1, QTIn-1, and granisetron overlapped in binding pocket show orientation difference of the two quaternary tropanes compared to granisetron and also distance from Arg 57. There is possiblity of change in orientation for QTpPy-1 and QTIn-1 towards Arg 57 due to their increase in binding affinity at *Ac* 5-HT_{3A} (2). PDB ID: 2YME.

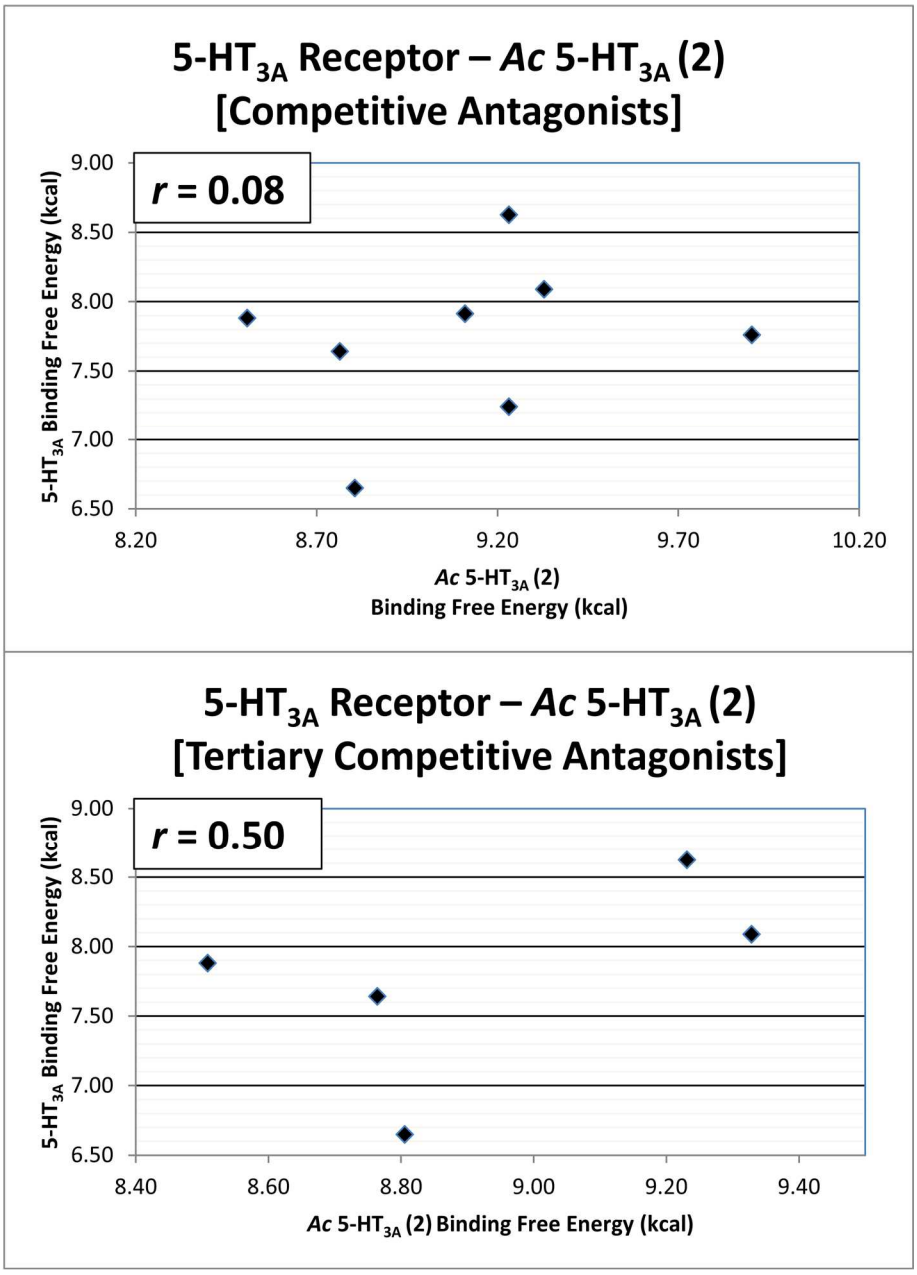

Figure 15. Correlation of 5-HT$_{3A}$ intact cell receptor binding free energy with *Ac* 5-HT$_{3A}$ (2) binding free energy

Conversion to Gibbs free energy was used to correlate the binding values of triazole compounds at 5-HT$_{3A}$ receptor and *Ac* 5-HT$_{3A}$ (2). K_d values were converted to free energy using the equation $\Delta G^{\circ} = -RT \ln K_d$ where R is the gas constant 1.98 cal/degree*mole and T is the absolute temperature (Taylor and Insel, 1990). Correlation was done using Microsoft Excel to obtain a Pearson correlation coefficient (r).

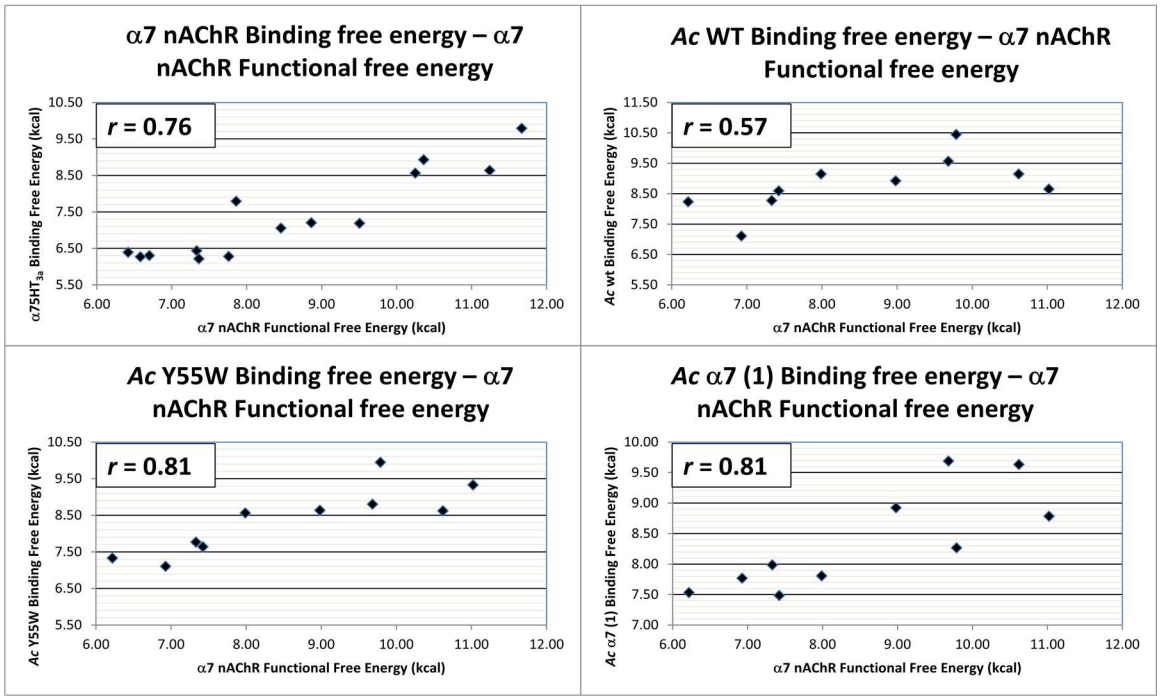

Figure 16.1. Correlation of α7 nAChR intact cell receptor functional free energy with α7 nAChR, *Ac* WT, *Ac* Y55W, and *Ac* α7 (1) binding free energy
Conversion to Gibbs free energy was used to correlate the functional values of triazole compounds at α7 nAChR with the binding values at α7 nAChR, *Ac* WT, *Ac* Y55W, and *Ac* α7 (1). K_d values were converted to free energy using the equation $\Delta G^{\circ} = -RT \ln K_d$ where *R* is the gas constant 1.98 cal/degree*mole and *T* is the absolute temperature (Taylor and Insel, 1990). Correlation was done using Microsoft Excel to obtain a Pearson correlation coefficient (*r*).

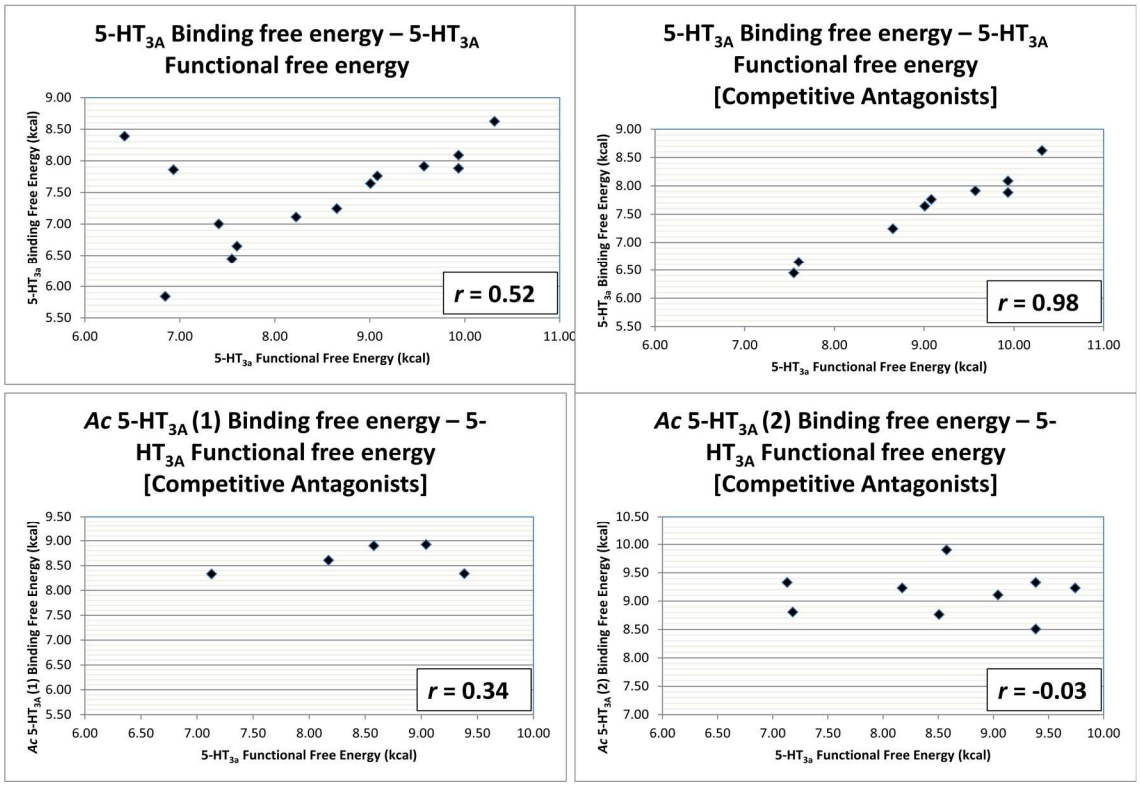

Figure 16.2. Correlation of 5-HT$_{3A}$ intact cell receptor functional free energy with 5-HT$_{3A}$ receptor, *Ac* 5-HT$_{3A}$ (1), and *Ac* 5-HT$_{3A}$ (2) binding free energy
Conversion to Gibbs free energy was used to correlate the functional values of triazole compounds at 5-HT$_{3A}$ receptor with the binding values at 5-HT$_{3A}$ receptor, *Ac* 5-HT$_{3A}$ (1), and *Ac* 5-HT$_{3A}$ (2). K_d values were converted to free energy using the equation $\Delta G^{\circ} = -RT \ln K_d$ where R is the gas constant 1.98 cal/degree*mole and T is the absolute temperature (Taylor and Insel, 1990). Correlation was done using Microsoft Excel to obtain a Pearson correlation coefficient (r).

III

DISCUSSION

Neuronal nicotinic acetylcholine receptors and serotonin receptors are distributed widely throughout the central nervous system and are key targets for potential therapeutic treatments for disorders of development and aging, such as schizophrenia and Alzheimer's disease. Because of the variety of subunits available for each family of receptor, it is pertinent to identify key determinants for receptor selectivity during the development of therapeutic agents.

Through a long standing collaboration with Dr. Barry Sharpless' lab and Valery Fokin's laboratories, an extensive library of triazole compounds were synthesized through *in situ* click chemistry. Of the compounds, 15 compounds selective for α7-nAChR and 5-HT_{3A} receptor were chosen for further characterization through functional and binding assays. Here, I used a medium throughput intact cell receptor binding assay to evaluate binding affinities of the compounds at the two receptors. I also characterized the functional activity of the ligands through a CNiFER-based fluorescent assay developed by a previous graduate student, and also conducted binding assays with acetylcholine binding proteins such as *Aplysia californica* (*Ac*) and its mutant variants as a prelude into examining structures of the complexes crystallographically.

The development of a intact cell receptor binding assay allowed me to investigate and quantifiably assess the effect of mutations at key residues of the binding pocket on ligand binding and selectivity. Along with functional and binding data, I was able to present a thorough picture of the characterization of the triazole compounds (Table 1-3). Using binding values and crystal structure analysis, I depicted the orientation of tertiary and quaternary tropanes in the

binding pocket and their position in the aromatic nest that determine their selectivity (Figure 6, 7). I have also conducted several correlation studies between intact cell receptor and AChBP binding data and used crystal structures to develop a rationale for differences in binding values (Figure 8, 9). Using an α7-similar *Ac* mutant constructed by another previous graduate student, I have shown a possible explanation behind the link between the presence of β*9*-10 linker mutations and selectivity of α7 nAChR against tertiary tropane compounds (Figure 10). Using two 5-HT_{3A}-similar mutants, I was able to show their effect on ligand selectivity and also the extent of their interaction with the triazole compounds through crystal structures (Figure 12, 14). Finally, I explained the relationship between binding and functional data through correlation studies (Figure 16).

Structural basis for strong affinity of quaternary tropane triazoles at α7-nAChR

Based on the binding and functional activity data of the receptors assayed, quaternary tropane triazoles at α7-nAChR have shown a 3 to 100-fold increase in affinity compared to their tertiary equivalents. Based on previous studies and crystal structures with AChBP, the increase can be explained by the cation-π interaction of the positively charged quaternary ammonium with the π-orbitals of an aromatic nest on the principal subunit of the receptor binding-pocket (Xiu et al., 2009). The principal subunit contains four key aromatic residues situated around the quaternary tropane: Tyr 93, Trp 147, Tyr 188, and Tyr 195. As shown

in Figure 6, Tyr 93, Trp 147, and Tyr 188 exhibit the strongest stabilizing interaction with the quaternary ammonium, showing a distance from the center of the aromatic ring to the quaternary nitrogen of 4.6-4.8 Å, which is noted to be adequate for strong cation-π interactions (Schärer et al., 2005). Of the three, Tyr 93 is likely to be the most stabilizing residue according to Figure 6, which reveals its aromatic ring's more optimal geometry (~10° to the normal) to the cation compared to the other two residues (~20° to the normal) (Marshall et al., 2009). Tyr 195, while too far away for optimal cation-π interaction at 6.4 Å, serves to surround the nitrogen and anchor the triazole through a series of hydrogen-bond linkage with surrounding water molecules (Grimster et al., 2012). The importance of this aromatic nest to quaternary tropane stabilization is also shown by their binding values at *Ac*. All four aromatic residues are conserved in *Ac*, and the binding results at *Ac* displayed a similar trend to that of α7 binding values with generally a 2 to 100-fold increase in affinity for quaternary tropanes compared to tertiary. These results identified the importance of the aromatic nest in establishing strong affinity with quaternary tropane compounds.

Structural basis for interaction of tertiary tropane triazoles at α7-nAChR

On the other hand, tertiary tropane triazoles have shown reduced affinity at α7 receptors. This reduced affinity can be largely explained by the tropane moiety's positioning in the binding pocket. The position of the tertiary tropane allows it to mainly interact with only two of the four residues in the aromatic nest: Trp 147 and Tyr 195. As the Figure 7 shows, both residues are strong stabilizers

for the tertiary ammonium with a distance of 4.4-4.5 Å and an adequate geometry of about 15-20° to the normal of the ring. The tertiary tropane is also oriented closer towards the amide backbone carbonyl of Trp 147 within hydrogen bonding distances (2.8 Å). This change reveals a 2.5 Å difference between the position of the tertiary tropane compared to the quaternary (2.8 Å vs 5.3 Å), showing the Trp 147 as having a stronger stabilizing effect for the tertiary tropane and also the general positional difference between the two tropane structures in the aromatic nest. It is also possible that structural differences in the β9-10 linker at the α7-nAChR could contribute to the reduced affinity of the tertiary tropanes by affecting the ability of Tyr 195 on the C loop to properly interact with the tertiary nitrogen.

Structural basis for reduced affinity of quaternary tropane triazoles at 5-HT_{3A} receptor

From both receptor binding and functional activity data, quaternary tropane triazoles at the 5-HT_{3A} receptor have shown reduced affinity (generally a 3 to 100-fold decrease) compared to their affinity at α7-nAChR. As noted previously, the affinity of the quaternary tropane in the binding pocket is dependent on its cation-π interaction with three key aromatic residues, Tyr 93, Trp 147, and Tyr 188, and also to a lesser extent, hydrogen bond stabilization by Tyr 195. However, in the 5-HT_{3A} receptor, Tyr 93 and Tyr 188 are replaced by Asn and Phe respectively, restricting the cation-π interactions to Trp 147 and a less electron-rich Phe 188 (Thompson and Lummis, 2006). These residue

changes help explain the reduction of affinity of these compounds at the 5-HT_{3A} receptor and give insight into designing for compound selectivity at these receptors.

Structural basis for increased affinity of tertiary tropane triazoles at 5-HT_{3A} receptor

Tertiary tropane triazoles at the 5-HT_{3A} receptor have shown increased affinity (a 2 to 8-fold increase for receptor binding and a 3 to 10-fold increase for functional activity) compared to their tertiary equivalents. Furthermore, in general, affinity of these compounds at the 5-HT_{3A} receptor are increased 10 to 100-fold compared to their affinity at α7-nAChR. This selectivity of 5-HT_{3A} receptor for tertiary tropanes can be explained by three factors. First, as previously noted, the tertiary ammonium is stabilized by two primary aromatic residues, Trp 147 and Tyr 195, both of which interact with the moiety through strong cation-π interaction (Figure 7). However, as shown in the α7-similar *Ac* mutant, *Ac* α7 (1), mutations in the β9-10 linker may affect the interaction of the C loop with the tertiary tropane and explain the lack of affinity of tertiary compounds at α7-nAChR. Second, the tertiary protonated amine is stabilized through optimal hydrogen bonding (~2.8 Å) with the backbone carbonyl group of Trp 147 similar to the *Ac* complexes with nicotine, epibatidine, and tropisetron (Celie et al., 2004, Hibbs et al., 2009). This stabilization, likely absent for quaternary tropanes at the 5-HT_{3A} receptor, may explain for the difference in affinity between tertiary and quaternary compounds at the receptor. Third, according to the 5-HT_{3A}-similar mutant in

Figure 14.1, the presence of Arg 57 in the 5-HT_{3A} complementary subunit (Gln in α7-nAChR) presents a region for strong cation-π interaction (~3.7 Å, ~23° to the normal of the indazole ring in granisetron) with the hydrophobic aromatic rings in the triazole series. The presence of this interaction in the 5-HT_{3A} receptor may explain for the increase in affinity of tertiary tropanes when compared to α7-nAChR.

AChBPs show limited correlation in binding values to α7 and 5-HT_{3A} receptors

AChBPs have long been used as structural surrogates for nicotinic acetylcholine receptors. However, they differ in ligand binding properties due to evolutionary distances, a lack of interconversion between resting, activated, or desensitized conformational states, and species-specific recognition properties that are distinctive from receptor subtypes (Hansen et al., 2005, Talley et al., 2006). As such, they should be regarded as unique pentameric LBDs in terms of binding properties. For this set of triazole compounds, I decided to create correlation plots to show a baseline comparison in binding affinities between the control AChBPs and receptors. Both wild-type *Ac* and *Ls* showed weak correlation to α7-nAChR. *Ac* displayed a Pearson correlation coefficient (*r*) of 0.25, while *Ls* displayed a slightly better 0.31 positive correlation (Figure 8.1). The AcY55W mutant improved on this correlation with an *r* of 0.54 through the mutation of Tyr 55 to Trp 55, increasing the positive correlation from wild-type *Ac* by more than 2-fold. For the 5-HT_{3A} receptor, all three AChBPs displayed weaker

and more negative correlation compared to α7. According to Figure 8.2, both wild-type *Ac* and AcY55W mutant show a negative correlation *r* of -0.46 to -0.48, while *Ls* show little correlation with an *r* of -0.13.

The difference in correlation between α7 and 5-HT_{3A} receptors with AChBPs can be understood through several explanations. First, as shown in Table 5, α7 receptor shows a 60.9% sequence similarity with wild-type *Ac* but only a 28.7% protein identity. For wild-type *Ls*, α7 receptor shows a 58.5% sequence similarity and only a 27.3% in protein identity. These values are lower for 5-HT_{3A}. 5-HT_{3A} receptor shows a 54.8% sequence similarity and 24.9% protein identity with *Ac*, and a 56.7% sequence similarity and 22.6% protein identity with *Ls*. These numbers show that neither of the AChBPs are exact replicas for α7-nAChR or 5-HT_{3A} receptor. Second, all three AChBPs have a conserved aromatic nest in its binding pocket in a similar way to the α7-nAChR. The four conserved aromatic residues, Tyr 93, Trp 147, Tyr 188, and Tyr 195, give stability to the quaternary tropanes through cation-π interaction, allowing AChBPs to display a similar trend in preference for quaternary tropane triazole over tertiary analogues at α7. Third, there are key differences in interaction between the complementary subunit face and the ligand's hydrophobic aromatic moiety. In wild-type *Ac* and AcY55W mutant, the presence of Met 116 on β6 has possibly a strong influence on ligand affinity and orientation in the binding pocket. The residue sits at 4.5-4.9 Å from the center of QTPh-12's and granisetron's aromatic rings at a geometry of ~30-33° to the normal; both of these values are in an appropriate range (~4.5 to 5.5 Å with 30-60° preference) for a strong sulfur-

aromatic interaction (Figure 9.1). This sulfur-aromatic interaction has been noted to be stronger than hydrophobic interaction by 1-1.5 kcal/mol and at specific distances, is enough to stabilize or disrupt ligand-receptor interactions (Valley et al., 2012). While the interaction is not fully understood, it has been shown to play a critical role in protein stabilization and protein-ligand interactions. Furthermore, the complementary subunit face of AChBPs lack key aromatic residues such as Tyr 56, Arg 57, Tyr 106, Tyr 108, and Tyr 118, which are all present in the 5-HT_{3A} receptor. Shown in a structure of mouse 5-HT_{3A} receptor (Figure 9.2), Tyr 56 and Tyr 118 in particular (both conserved in the human 5-HT_{3A} receptor) are likely to participate in hydrogen bonding with the carbonyl linker and indazole of granisetron (Hassaine et al., 2014). Arg 57 is also important in establishing stability for this set of triazole compounds in the 5-HT_{3A} binding pocket.

Due to this lack of correlation between ligand-gated ion channel receptor and AChBP binding, one recent approach is to mutate AChBPs toward specific receptors in order to gather additional structural information and understand receptor's binding modes through these mutants. Drawing on information from two recent studies, I mutated wild-type *Ac* towards α7-nAChR in mutant *Ac* α7 (1) and wild-type *Ac* towards 5-HT_{3A} - receptor in mutants *Ac* 5-HT_{3A} (1) and *Ac* 5-HT_{3A} (2) (Nemecz and Taylor, 2011, Kester et al., 2012).

Structural analysis and rationale of triazole binding at the α7-similar *Ac* α7 (1) mutant

Based on the work of a previous graduate student in the Taylor lab, Akos Nemecz, I looked at two mutants, mutant II and III, which had the greatest sequence similarity and protein identity to α7-nAChR (Table 5). Ultimately, due to the instability of mutant II and its sensitivity to acidic conditions, I chose to use mutant III (designated as *Ac* α7 (1) for the purpose of this thesis) as the AChBP mutant for the triazole study (Nemecz and Taylor, 2011). The key difference between the two mutants was the lack of a set of β9-10 linker mutations (Q186R, H187F, S189E, P192K, and I196P) in mutant II which is likely to have contributed to its lack of stability.

Overall, binding affinities of the quaternary tropane triazoles do not deviate far from the values found in wild-type *Ac*. QTTh-1 and QTPh-12 showed the high affinity, improving upon the wild-type *Ac* values slightly, while QTmN-1 showed the largest deviation with a ~40-fold decrease in affinity (0.68 μM vs 0.016 μM). The average binding free energy (calculated from K_d) of the quaternary compounds showed a decrease of 0.65 kcal/mol, signifying an overall loss of affinity for the quaternary compounds. On the other hand, the binding of affinities of tertiary tropane triazoles displayed a larger difference. Out of the seven tertiary compounds, only TTTh-1 displayed an increase in affinity while four others did not pass the initial "quickscreens" (K_d represented as 5 μM or greater), showing a substantial decrease in affinity with *Ac* α7 (1). If we assumed these four compounds to have at least a K_d of 5 μM, we would find that the average binding free energy of the tertiary compounds to decrease by a substantial 1.1 kcal/mol,

signifying an overall close to 10-fold loss of affinity for the tertiary compounds at this mutant.

This substantial loss of affinity for the tertiary tropanes mirrored the similar loss of affinity of tropisetron at *Ac* α7 (1). Tropisetron, which also contained a tertiary tropane, is both a selective α7-nAChR agonist and 5-HT_{3A} antagonist. Its affinity was decreased by ~7-fold at *Ac* α7 (1) compared to *Ac* WT (730 nM vs 109 nM) and mutant II (730 nM vs 100 nM) (Nemecz and Taylor, 2011). This difference at *Ac* WT, especially when compared with mutant II, signified the importance of the mutations at the β9-10 linker in establishing a dramatic loss of affinity for tropisetron and similar tertiary tropane compounds.

A possible explanation for this loss of affinity may be the interaction between the C loop with D and F loops. As mentioned in previous studies, the C loop is crucial in agonist binding and ligand gating mechanisms – the loop tightens upon agonist binding, closing upon the ligand and initiating a fulcrum-like motion that causes the Cys-loop to move away from the pore, opening it for ion passage (Stober and Abrams, 2011). Thus, Cα distances between certain residues on C loop and the complementary subunit are correlated with partial agonism, full agonism, and antagonism. According to research on insect nAChR, MD simulations have shown that movement of the C loop can be altered through mutation of certain residues at the D or F loops (Selvam et al., 2015). In particular, the modification of Gln 57 to Lys 57 resulted in electrostatic interaction with neighboring residues, Asp 164 and Gln 189. This interaction caused the C loop to move away from the complementary subunit, opening up the binding site,

leading to less favorable interaction with the ligand, which depends on close interaction with residues at the C loop (Selvam et al., 2015). Furthermore, Gln 189 has shown to interact with Asp 164 and Thr 36 through hydrogen bonding, tightening the C loop towards the binding site. However, the S189E mutation in *Ac* α7 (1) alters the interaction of the C loop with Asp 164 and potentially other residues at the D or F loops (Figure 10). The electrostatic repulsion between the Glu 189 and Asp 164 along with the potential loss of important hydrogen bonding effects may cause the C loop to be more open during agonist binding. Previous studies have shown a similar orientation of the C loop in homology modeling of imidacloprid binding at α4β2, where we see a dramatic change in the orientation of the C loop upon mutation of Glu 189 (Glu 219 in α4β2) to a non-charged residue or mutation of a D loop residue Gln 57 (Thr 77 in α4β2) to a positively charged residue such as Arg. Upon mutating to a favorable electrostatic state, the C loop initiates a greater movement towards the D and F loops, resulting in stronger imidacloprid binding and response. These electrostatic differences and consequent C loop movement in *Ac* α7 (1) mutant might account for weaker tertiary tropane binding since, as previously discussed, the Tyr 193 on the C loop is crucial for stabilizing the tertiary tropane ring. (Toshima et al., 2009)

Correlation studies of *Ac* α7 (1) with the α7-nAChR receptor binding values yielded a small improvement from wild-type *Ac* (0.47 vs 0.25) and a comparable coefficient with the *Ac* Y55W mutant (0.47 vs 0.54) (Figure 8.1, 11).

Structural analysis and rationale of triazole binding at the 5-HT_{3A}-similar *Ac* 5-HT_{3A} (1) mutant

Based on the research of an international collaboration published in 2013, I identified and chose two 5-HT_{3A}-similar *Ac* mutants, *Ac* 5-HT_{3A} (1) and *Ac* 5-HT_{3A} (2), which had closest affinities in terms of 5-HT and granisetron binding to the 5-HT_{3A} receptor (Kesters et al., 2012). Both mutants contained 4 mutations, 3 of them conserved. Unique to *Ac* 5-HT_{3A} (1) was the Y55W mutation, while *Ac* 5-HT_{3A} (2) contained the Q57R mutation.

Overall, the binding affinities of the triazole series at *Ac* 5-HT_{3A} (1) reflected very similar affinities to the values at *Ac* Y55W, but they also showed improved correlation with the 5-HT_{3A} receptor. According to the correlation studies (Figure 13), we see a 0.83 positive correlation with the affinities at *Ac* Y55W, but we also see a 0.45 positive correlation with the 5-HT_{3A} receptor, a significant improvement from initial correlation of *Ac* by 0.78, showing the impact of the Trp 55 mutation in affecting the affinity of the triazole compounds in the pocket. Furthermore, *Ac* 5-HT_{3A} (1)'s high correlation with *Ac* Y55W signified the effect of peripheral mutations in the mutant; S94E, V142L, and K143T were, as predicted, primarily mutations to preserve structural stability and were too distant from the binding pocket to effect significant change in ligand affinity. It should be noted however that the new E94-T143 complex establishes greater stability between the A and B Loops through a strong electrostatic interaction, which may have effect on the general flexibility of the principal subunit.The key residue mutated in *Ac* 5-HT_{3A} (1) is Tyr 55 to Trp 55 on the D Loop, introducing a

hydrophobic indole side chain that has shown to interact through hydrophobic or cation-π interactions with various agonists at both α7 and 5-HT_{3A} receptors and is critical in receptor gating and desensitization (Gay et al., 2007).

The improved correlation with the 5-HT_{3A} receptor is likely due to the loss of affinity of the quaternary tropanes in the mutant. The average binding free energy of the quaternary tropanes is decreased by 0.32 kcal/mol, and each quaternary tropane except for QTIn-1 lost affinity compared to the affinities at wild-type *Ac*. Similarly, I found the tertiary tropanes to lose significant affinity due to the mutation – 4 out of the 7 tertiary compounds failed to past the "quickscreen" at a K_d cut-off of 5 μM. While this loss of affinity seem to conflict with previous studies on the importance of Trp 55's cation-π effect in both α7 and 5-HT_{3A} agonist binding, it fits with the orientation of the triazole compounds in the binding pocket. Unlike smaller compounds such as 5-HT_{3A}, the triazole series share similar characteristics with larger antagonist like granisetron, which has been shown to not be strongly affected by Trp 55 due to the positioning of its tropane nitrogen in Figure 12, which is out of range (6.6 Å) for cation-π interaction with the tryptophan (Spier and Lummis, 2000, Kesters et al., 2012). Furthermore, there is a possibility that the Tyr 55 in wild-type *Ac* confers a degree of stability to the triazole series through a hydrogen bonding complex between the tyrosine hydroxyl group and the triazole linker.

Interestingly, QTIn-1 with *Ac* Y55W (Figure 12) shows the quaternary ammonium of the tropane to be in cation-π proximity with the Trp 55 at a distance of 4.3 Å, which is further confirmed by its gain in affinity at *Ac* 5-HT_{3A} (1) by ~3-

fold. This orientation appears to be unique amongst the quaternary compounds since QTIn-1 is the only compound to show increase in affinity. It would be interesting to investigate crystallographically and understand the extent of the effect of the indole moiety of QTIn-1 on the positioning of the tropane ring in the aromatic nest.

Structural analysis and rationale of triazole binding at the 5-HT$_{3A}$-similar *Ac* 5-HT$_{3A}$ (2) mutant

The binding affinities of triazole series at *Ac* 5-HT$_{3A}$ (2) revealed increased affinity for 13 of 15 compounds compared to wild-type *Ac*. The average binding energy is increased by 0.42 kcal/mol for the quaternary tropanes and 0.67 kcal/mol for the tertiary analogues. The most potent quaternary compounds were QTmN-1, QTIn-1, and QTTh-1 with K_d's of 13 nM, 23 nM, and 41 nM respectively, while QTIn-1 displayed the greatest increase in affinity from wild-type *Ac* of about 10-fold, the only quaternary compound to show more than a 1.5- to 2-fold difference. Generally, except for QTIn-1, the majority of the quaternary compounds showed only slight increases in binding affinity compared to the wild-type. On the other hand, the majority of tertiary compounds displayed a consistency in their increase in affinity. Out of the 7 tertiary compounds, 4 of the compounds showed an increase of 3 to 5-fold in binding affinity, and the most potent tertiary, TTTh-1, showed a dramatic increase from over 5 μM to 0.11 μM, which was at least a 50-fold increase. This comparison serves to demonstrate

the mutant's selective and consistent increase in affinity for tertiary tropanes, while its effects on quaternary compounds appear minimal aside from QTIn-1.

According to Figure 15, the correlation charts show a similar story. The correlation coefficient for competitive antagonists at *Ac* 5-HT_{3A} (2) compared to the 5-HT_{3A} receptor is 0.08, showing almost zero correlation in affinities with the receptor. However, it becomes clearer when the antagonists are separated into quaternary and tertiary. Quaternary antagonists only achieved a low 0.18 positive correlation, while the tertiary antagonists achieved a 0.50 positive correlation, which is a 0.73 positive increase from the correlation data of tertiary antagonists between wild-type *Ac* and 5-HT_{3A} receptor. This difference in correlation confirms the mutant's role in creating a more 5-HT_{3A}-selective binding pocket for tertiary tropane triazoles.

As previously discussed, several of *Ac* 5-HT_{3A} (2)'s mutations, S94E, V142L, and K143T, are primarily structural mutations necessary to maintaining the stability and integrity of the subunit. The key residue in *Ac* 5-HT_{3A} (2) is Arg 57 on the D Loop, an amino acid with a positively charged side chain that allows it to interact with aromatic ligands through cation-π interaction. This interaction can be observed in Figure 14.1 in which the aromatic center of granisetron's indazole is positioned 3.6-4.6 Å away from Arg 57's positively charged guanidium side chain and ~23-33° from the normal of the indazole. Figure 14.2 shows the difference in position between granisetron and quaternary compound, QTpPy-1; due to the positioning of its tertiary tropane ring, granisetron's indazole is situated closer to Arg 57 than QTpPy-1's *para*-positioned pyridine moiety, making the

cation-π interaction more important for the stabilization of compounds with tertiary tropanes. When I compared the difference in K_d between the different aromatic moieties of tertiary compounds with previous computational studies of electrophilic aromatic substitution on cation-π interaction, I found some general correlations (Ma and Dougherty, 1997). The phenyl and indole tertiary compounds had strong affinities, 0.13 μM and 0.23 μM respectively. They were both more potent than the methoxynaphthalene at 0.34 μM presumably due to the lack of an electron-withdrawing effect in the bicyclic ring. They were also more potent than the pyridine series, which fits previous studies explaining the localization of electrostatic potential towards the amine and away from the center of the aromatic ring and resulting in a weaker cation-π interaction (Ma and Dougherty, 1997). However, this rationale fails to explain the potent binding of the five-membered thiophene (0.11 μM), since we would expect to find a similar weak cation-π interaction at the thiophene. A plausible explanation for this value is orientation angle of the thiophene towards Arg 57 due to the inflexibility of the triazole-thiophene linker. In that case, the positive charge of Arg 57 could be interacting with the concentrated electron cloud of the thiophene's sulfur rather than the center of the thiophene ring, resulting in a substantially stronger cation-π interaction.

Three interesting things were of note about the triazole series' interaction with *Ac* 5-HT_{3A} (2). First, NTPh-2, the only secondary tropane triazole in the series, showed a K_d of 0.49 μM at *Ac* 5-HT_{3A} (2). This is important because not only is *Ac* 5-HT_{3A} (2) the only AChBP to have significant (submicromolar) affinity

for NTPh-2, its affinity for the triazole is also nearly identical to 5-HT_{3A} receptor's affinity to the compound (0.51 μM). This observation suggests an important necessity of Arg 57 to stabilize NTPh-2 in the binding pocket. Second, the impact of the methionine at 116 (Figure 14.1) on granisetron's aromatic moiety is unclear. The distance from its sulfur to granisetron's indazole center is 5.3 Å at ~40° to the normal of the ring, which, as previously mentioned, could allow it to engage in sulfur-aromatic interaction. Third, the binding orientation of QTIn-1 in the mutant is unclear. In Figure 14.2, the indole moiety's orientation in the wild-type's pocket contradicts the impact of the Q57R mutation on the compound's binding affinity. The change to Arg 57 clearly showed a ~10-fold increase in affinity (0.35 μM to 0.023 μM) even though the indole is distant from the residue in wild-type *Ac*. This observation suggests a greater degree of flexibility of QTIn-1 in the pocket compared to other quaternary compounds and also the indole's shift towards Arg 57 due to the strong cation-π interaction.

Relationship of binding affinity with functional activity of triazole compounds

It is important to consider the role of efficacy in transducing ligand occupation into the stimulus, which in this case is agonist response of the receptor. The range of efficacy for different ligands may be large and could account for different capacity of agonists or antagonists in creating a response from fractional occupation (Taylor and Insel, 1990). This idea is relevant when examining agonist response at α7-nAChR and binding affinity. Correlation

between the functional and binding values for the triazole series at α7-nAChR gave an *r* of 0.76, demonstrating a difference between receptor occupation and agonist response (Figure 16.1). As expected, wild-type *Ac* showed a weaker correlation *r* of 0.57 with the agonist response at α7. This correlation is improved at *Ac* Y55W and *Ac* α7 (1) mutants, reaching an *r* of 0.81, which demonstrates the importance of Trp 55 in conferring selectivity for α7 agonists.

When examining the antagonist properties of the triazole series at 5-HT_{3A} receptor, there was a stronger correlation between the binding and functional values. When I refined the correlation down to competitive antagonists, the correlation showed an r of 0.98, signifying a strong positive correlation very close to 1 and thus the direct relationship between receptor occupation and competitive antagonism (Figure 16.2). This is to be expected for competitive antagonists since they directly compete with agonists for receptor binding. This correlation is comparatively weaker for both *Ac* 5-HT_{3A} mutants – 0.34 for *Ac* 5-HT_{3A} (1) and -0.03 for *Ac* 5-HT_{3A} (2). However, these are still significant improvements upon correlations of competitive antagonists at wild-type *Ac* (*r* = -0.24).

Future direction and potential drug design insights

In conclusion, while my experiments provide insight into structural selectivity of α7-nAChR and 5-HT_{3A} receptor, further information from additional crystallography studies can help bolster my rationales and explain some of the areas that are difficult to understand. Specifically, it would be useful to crystallize *Ac* α7 (1) with both quaternary and tertiary agonists since it will help determine

how the β9-10 linker mutations contribute to the ligand's selectivity. It would be also interesting to mutate additional residues in the 5-HT_{3A}-similar mutants to see if it's possible to get better correlations in binding at the receptor. Potential residues to mutate to include Tyr 56, Tyr 106, Tyr 108, and Tyr 118, which are on the complementary subunit and can potentially engage in hydrogen-bonding interaction with the triazole or the aromatic moiety.

In terms of drug design, the conserved nature of the α7-nAChR aromatic nest causes difficulty in creating potent yet selective compounds for the receptor. One method in creating more selective α7 ligands is to modify the tropane moiety to another amine ring system that is optimized to cation-π interact with Tyr 93 and Tyr 188, both of which are not present in the 5-HT_{3A} receptor. Kuntarat Arunrungvichian, a former traveling scholar at our lab, has worked on synthesizing new α7-nAChR selective compounds based around TTIn-1, and she has found success in enhancing selectivity by replacing the tropane ring with piperidine, pyrrolidine, or azepane (unpublished data). Furthermore, since the Arg 57 residue is important for achieving strong binding at the 5-HT_{3A} pocket, modifications could be done at the hydrophobic aromatic moiety to create a stronger cation-π interaction while maintaining a preference for the 5-HT_{3A} receptor by keeping the tertiary tropane. Possible modfications include using bicyclic ring systems similar indole with strong negative surface charge that could interact effectively with the Arg 57 residue. Adding carbon linkers between the triazole and the aromatic ring could also affect this cation-π interaction by increasing the degree of flexibility of its positioning in the pocket.

IV

METHODS AND MATERIALS

Cell Culture

Cells were cultured in 10 cm plates with Dulbecco's modified Eagle medium (DMEM) enriched with 10% fetal bovine serum (FBS) and 1% glutamine and incubated at 37°C in 10% CO_2 conditions.

I employed a stable cell line with cell-based neurotransmitter fluorescently engineered reporter (CNiFER) expressed TN-XXL, genetically-encoded Ca2+ sensor. The CNiFER cell line expressing human $\alpha4\beta2$-nAChR were prepared by cotransfecting human $\alpha4$ and $\beta2$ cDNAs into human embryonic kidney (HEK) tsA201 cells and then selecting for $\alpha4$ expression via Zeocin (0.5 mg/mL from Invitrogen) and $\beta2$ expression via G418 (0.6 mg/mL from Invitrogen). CNiFER cell lines expressing human $\alpha7$-nAChR, mouse 5-HT_{3A} serotonin receptors, or $\alpha7$/5-HT_{3A} chimaeric nAChR were similarly generated by calcium phosphate transfection of cDNA gene into TN-XXL control cells. The latter two were generated in HEK293 cells expressing TN-XXL. (Yamauchi et al., 2011)

Stable cell lines expressing AChBPs (*Ls*, *Ac*, *Ac* Y55W, *Ac* $\alpha7$ (1), *Ac* 5-HT_{3A} (1), and *Ac* 5-HT_{3A} (2)) were generated by calcium phosphate transfection of AChBP FLAG tagged DNA into HEK293S cells lacking the N-acetyglucosaminyltransferase I ($GNTI^-$) gene (Reeves et al., 2002). Cells expressing appreciable AChBP were selected with G418 (0.6 mg/mL), and the proteins were purified with FLAG-antibody resin (Sigma) and FLAG-peptide (Sigma) as an eluent.

Radioligand nAChR: Intact Cell Binding Assay

CNiFER cell lines expressing nAChRs were harvested at 70-80% confluency using trypsin and diluted with Hank's Balanced Salt Solution (HBSS) buffer with 1% BSA until a cell count ranging from 100,000 to 200,000 per 20 mL was reached. The resulting solution was then plated into a 96-well low-profile plate, filling each well to a volume of 0.02 mL. Radioligands, (±)-[^{3}H] epibatidine or (±)-[^{3}H] granisetron (both PerkinElmer), wheat germ agglutinin scintillation proximity assay (SPA) beads (100 μg/well) (Amersham Biosciences), and different concentrations of competing ligands diluted with HBSS buffer (1% BSA) were added to the cell solution in each well, filling each well to a final volume of 0.08 mL (Berry and Price-Jones, 2005). The plates were incubated at room temperature for 2 hours before insertion into a Wallac 1450 Microbeta Trilux to run for 8 times with 2 hours in between runs.

The data were analyzed using GraphPad Prism 4 and fitted to a sigmoidal dose-response curve (variable slope) to determine the IC_{50} and K_d values.

Radioligand AChBP Binding Assay

AChBP (0.5 nM final concentration in binding sites) was prepared with polyvinyltoluene anti-mouse SPA scintillation beads (12 μg/well) (Amersham Biosciences) and anti-FLAG M2 mouse antibody (Sigma) (Talley et al., 2006). This solution was then plated onto a 96-well low-profile plate with different concentrations of competing ligands diluted in 0.1M $NaPO_4$ buffer. After a 15

minute incubation, radioligands, (±)-[^{3}H] epibatidine or (±)-[^{3}H] granisetron, were added into each well, filling each well to a final volume of 0.048 mL. The plates were incubated at room temperature for 1 hour before insertion into a Wallac 1450 Microbeta Trilux to run for 2 times with no additional incubation in between runs.

The data were analyzed using GraphPad Prism 4 and fitted to a sigmoidal dose-response curve (variable slope) to determine the IC_{50} and K_d values.

CNiFER-based Flex Assay

CNiFER cell lines expressing nAChRs were selected at 60-80% confluency and plated at 100 uL volume per well into TC treated 96-well plates. They were then treated with 50 μL of 0.1 mg/mL poly-D-lysine for 30 minutes and then washed with Dulbecco's phosphate buffered saline (DPBS). After overnight incubation at 37°C in 10% CO_2 conditions, media in each well was replaced with 100 μL of artificial cerebral spinal fluid (aCSF) buffer along with competitive antagonists or positive allosteric modulators (PAM) and incubated for 30 minutes at 37°C before running on the Molecular Devices FlexStation III instrument (Yamauchi et al., 2011).

Mean peak FRET ratios were calculated from replicates (2 to 3 per point) using SoftMax Pro 5.4 (Molecular Devices) and plotted against agonist concentrations using GraphPad Prism 4. Sigmoidal dose-response (variable slope) regression analysis of the mean peak FRET ratios were used to generate

a dose-response curve in order to obtain an EC_{50} value. In the case of competitive antagonists, antagonist-dependent shifts in EC_{50} values were used to calculate the dose ratios which were then used to calculate the K_d values (Taylor and Insel, 1990, Arunlakshana and Schild 1959).

Mutagenesis

Ac WT cDNA was mutated using the overlap extension PCR method (Nemecz and Taylor, 2011). Primers including the desired mutations were designed and created fragments of mutated *Ac* cDNA after PCR. A second PCR with each of the fragments created a complete mutated *Ac* construct with the desired mutations. The PCR product was digested using restriction enzymes HindIII and XbaI, isolated using gel eletrophoresis, and extracted from the agarose gel using a gel extraction kit (Qiagen). The insert was then ligated into a digested pFlag-CMV-3 vector (Sigma) using T4 DNA ligase (New England Biolabs) and transformed into competent DH5α cells. The transformed colonies were selected by ampillicin resistance. The mutant plasmids were purified using a miniprep kit (Qiagen) and sent to Retrogen for sequencing.

Calcium Phosphate Transfection

HEK293S GNTI$^-$ cells were plated onto 6-well plates 1 or 2 days prior to transfection such that each plate had 50-70% confluency at time of transfection.

2.5 M $CaCl_2$, dH_2O, and 2-5 μg of cDNA were prepared in solution, mixed into 2X HEPES transfection buffer, and left to stand for 25-45 minutes until they became slightly opaque in appearance. The solution was then injected into the 6-well plates containing the HEK cells and left to incubate at 37°C in 10% CO_2 conditions for 12-16 hours before changing media. Transient cells were allowed to undergo 1-3 days of protein expression before experimentation.

Protein Expression and Purification

Stable cell lines expressing desired AChBP were generated using G418 (0.6 mg/mL) selection in HEK293S GNTI- cells. Once 80-90% confluency had been reached on the 10 cm plates, the cells were transferred to multilayer flasks and maintained with DMEM enriched with 2% FBS and 1% glutamine at 37°C in 10% CO_2 conditions. Protein expressed in media was harvested every 3-4 days and purified using an affinity column containing FLAG-antibody resin. FLAG-peptide diluted in filtered TBSA buffer (50 mM Tris-HCl, pH 7.5, 140 mM NaCl, and 0.02% NaN_3) was used for eluting FLAG-tagged protein. The concentration of the purified protein was determined using a Thermo Scientific Nanodrop 2000c spectrophotometer based on the molecular weight of the monomeric form and the extinction coefficient of the AChBP.

Fast Protein Liquid Chromatography

Fast protein liquid chromatography (FPLC) was used both for analyzing the purify of the protein and for separating the pentameric AChBP species from its monomeric form. 10 μg of desired protein in filtered TBSA was run through a Superose 6 10/300 GL column. Results displaying a 15-20 mAU peak at a range of 15-16.5 mL indicate the presence of purified pentameric AChBP, separated from any monomeric impurities.

Crystallography

AChBP crystals were picked to be screened for diffraction at the Advanced Light Source Synchrotron in Berkeley, California. CCP4i and Phenix were used to refine the structure data. Several structures were taken from the Protein Data Bank, and both Coot and Pymol were used to manipulate the structures. The images were produced using Pymol. (Nemecz and Taylor, 2011)

REFERENCES

Arunlakshana, O., & Schild, H. O. (1959). Some quantitative uses of drug antagonists. *British Journal of Pharmacology and Chemotherapy, 14*(1), 48-58.

Bencherif, M., Stachowiak, M. K., Kucinski, A. J., & Lippiello, P. M. (2012). Alpha7 nicotinic cholinergic neuromodulation may reconcile multiple neurotransmitter hypotheses of schizophrenia. *Medical Hypotheses, 78*(5), 594-600.

Berry, J., & Price-Jones, M. (2005). Measurement of radioligand binding by scintillation proximity assay. In A. Davenport (Ed.), (pp. 121-138) Humana Press.

Bouzat, C. (2012). New insights into the structural bases of activation of cys-loop receptors. *Journal of Physiology-Paris, 106*(1–2), 23-33.

Brejc, K., van Dijk, W. J., Klaassen, R. V., Schuurmans, M., van, d. O., Smit, A. B., et al. (2001). Crystal structure of an ACh-binding protein reveals the ligand-binding domain of nicotinic receptors. *Nature, 411*(6835), 269-276.

Celie, P. H., S. E. van Rossum-Fikkert, et al. (2004). "Nicotine and carbamylcholine binding to nicotinic acetylcholine receptors as studied in AChBP crystal structures." *Neuron* 41(6): 907-14.

Gay, E. A., Giniatullin, R., Skorinkin, A., & Yakel, J. L. (2007). Aromatic residues at position 55 of rat α7 nicotinic acetylcholine receptors are critical for maintaining rapid desensitization. *The Journal of Physiology, 586*, 1105-1115.

Grimster, N. P., Stump, B., Fotsing, J. R., Weide, T., Talley, T. T., Yamauchi, J. G., et al. (2012). Generation of candidate ligands for nicotinic acetylcholine receptors via in situ click chemistry with a soluble acetylcholine binding protein template. *Journal of the American Chemical Society, 134*(15), 6732-6740.

Hansen, S. B., Sulzenbacher, G., Huxford, T., Marchot, P., Taylor, P., & Bourne, Y. (2005). Structures of aplysia AChBP complexes with nicotinic agonists and antagonists reveal distinctive binding interfaces and conformations. *The EMBO Journal, 24*(20), 3635-3646.

Hassaine, G., Deluz, C., Grasso, L., Wyss, R., Tol, M. B., Hovius, R., et al. (2014). X-ray structure of the mouse serotonin 5-HT3 receptor. *Nature, 512*(7514), 276-281.

Hibbs, R. E., Sulzenbacher, G., Shi, J., Talley, T. T., Conrod, S., Kem, W. R., et al. (2009). Structural determinants for interaction of partial agonists with

acetylcholine binding protein and neuronal α7 nicotinic acetylcholine receptor. *The EMBO Journal, 28*(19), 3040-3051.

Hodge, C. W., Kelley, S. P., Bratt, A. M., Iller, K., Schroeder, J. P., & Besheer, J. (2004). 5-HT3A receptor subunit is required for 5-HT3 antagonist-induced reductions in alcohol drinking. *Neuropsychopharmacology : Official Publication of the American College of Neuropsychopharmacology, 29*(10), 1807-1813.

Jensen, A. A., FrÃ¸lund, B., Liljefors, T., & Krogsgaard-Larsen, P. (2005). Neuronal nicotinic acetylcholine receptors: structural revelations, target identifications, and therapeutic inspirations. *Journal of Medicinal Chemistry, 48*(15), 4705-4745.

Kalamida, D., Poulas, K., Avramopoulou, V., Fostieri, E., Lagoumintzis, G., Lazaridis, K., et al. (2007). Muscle and neuronal nicotinic acetylcholine receptors. *FEBS Journal, 274*(15), 3799-3845.

Kesters, D., Thompson, A. J., Brams, M., van Elk, R., Spurny, R., Geitmann, M., et al. (2012). Structural basis of ligand recognition in 5-HT(3) receptors. *EMBO Reports, 14*(1), 49-56.

Kolb, H. C., & Sharpless, K. B. (2003). The growing impact of click chemistry on drug discovery. *Drug Discovery Today, 8*(24), 1128-1137.

Lummis, S. C. R. (2012). 5-HT3 receptors. *Journal of Biological Chemistry, 287*(48), 40239-40245.

Ma, J. C., & Dougherty, D. A. (1997). The cation-π interaction. *Chemical Reviews, 97*(5), 1303-1324.

Marshall, M. S., Steele, R. P., Thanthiriwatte, K. S., & Sherrill, C. D. (2009). Potential energy curves for cation-π interactions: Off-axis configurations are also attractive. *The Journal of Physical Chemistry A, 113*(48), 13628-13632.

Nemecz, A., & Taylor, P. W. (2011). Creating an a7 nicotinic acetylcholine recognition domain from the acetylcholine binding protein: Crystallographic and ligand selectivity analyses. *Journal of Biological Chemistry,*

Parri, H. R., Hernandez, C. M., & Dineley, K. T. (2011). Research update: Alpha7 nicotinic acetylcholine receptor mechanisms in alzheimer's disease. *Biochemical Pharmacology, 82*(8), 931-942.

Rucktooa, P., Smit, A. B., & Sixma, T. K. (2009). Insight in nAChR subtype selectivity from AChBP crystal structures. *Biochemical Pharmacology, 78*(7), 777-787.

Schärer, K., Morgenthaler, M., Paulini, R., Obst-Sander, U., Banner, D. W., Schlatter, D., et al. (2005). Quantification of cation-π interactions in protein-ligand complexes: Crystal-structure analysis of factor xa bound to a quaternary ammonium ion ligand. *Angewandte Chemie International Edition, 44*(28), 4400-4404.

Selvam, B., Graton, J., Laurent, A. D., Alamiddine, Z., Mathé-Allainmat, M., Lebreton, J., et al. (2015). Imidacloprid and thiacloprid neonicotinoids bind more favourably to cockroach than to honeybee α6 nicotinic acetylcholine receptor: Insights from computational studies. *Journal of Molecular Graphics and Modelling, 55*(0), 1-12.

Spier, A. D., & Lummis, S. C. R. (2000). The role of tryptophan residues in the 5-Hydroxytryptamine3 receptor ligand binding domain. *Journal of Biological Chemistry, 275*(8), 5620-5625.

Stober, S. T., & Abrams, C. F. (2011). Enhanced meta-analysis of acetylcholine binding protein structures reveals conformational signatures of agonism in nicotinic receptors. *Protein Science : A Publication of the Protein Society, 21*(3), 307-317.

Talley, T. T., Yalda, S., Ho, K., Tor, Y., Soti, F. S., Kem, W. R., et al. (2006). Spectroscopic analysis of benzylidene anabaseine complexes with acetylcholine binding proteins as models for Ligandâ€“Nicotinic receptor interactions. *Biochemistry, 45*(29), 8894-8902.

Taylor, P. and P. A. Insel (1990). Molecular basis of pharmacologic selectivity . Chapter 1. *Principles of drug action : the basis of pharmacology. 3rd Ed.* W. B. Pratt and P. Taylor. New York, Churchill Livingstone**:** 1-102.

Thompson, A. J., & Lummis, S. C. R. (2006). 5-HT(3) receptors. *Current Pharmaceutical Design, 12*(28), 3615-3630.

Thompson, A. J., & Lummis, S. C. R. (2007). The 5-HT3 receptor as a therapeutic target. *Expert Opinion on Therapeutic Targets, 11*(4), 527-540.

Toshima, K., Kanaoka, S., Yamada, A., Tarumoto, K., Akamatsu, M., Sattelle, D. B., et al. (2009). Combined roles of loops C and D in the interactions of a neonicotinoid insecticide imidacloprid with the α4β2 nicotinic acetylcholine receptor. *Neuropharmacology, 56*(1), 264-272.

Tsetlin, V., Kuzmin, D., & Kasheverov, I. (2011). Assembly of nicotinic and other cys-loop receptors. *Journal of Neurochemistry, 116*(5), 734-741.

Unwin, N. (2005). Refined structure of the nicotinic acetylcholine receptor at 4 Å resolution. *Journal of Molecular Biology, 346*(4), 967-989.

Valley, C. C., Cembran, A., Perlmutter, J. D., Lewis, A. K., Labello, N. P., Gao, J., et al. (2012). The methionine-aromatic motif plays a unique role in stabilizing protein structure. *The Journal of Biological Chemistry, 287*(42), 34979-34991.

Xiu, X., Puskar, N. L., Shanata, J. A. P., Lester, H. A., & Dougherty, D. A. (2009). Nicotine binding to brain receptors requires a strong cation-π interaction. *Nature, 458*(7237), 534-537.

Yamauchi, J. G., Gomez, K., Grimster, N., Dufouil, M., Nemecz, Á., Fotsing, J. R., et al. (2012). Synthesis of selective agonists for the α7 nicotinic acetylcholine receptor with in situ click-chemistry on acetylcholine-binding protein templates. *Molecular Pharmacology, 82*(4), 687-699.

Yamauchi, J. G., Nemecz, Ã., Nguyen, Q. T., Muller, A., Schroeder, L. F., Talley, T. T., et al. (2010). Characterizing ligand-gated ion channel receptors with genetically encoded Ca(++) sensors. *Plos One, 6*(1), e16519.

Young, J. W., & Geyer, M. A. (2013). Evaluating the role of the alpha-7 nicotinic acetylcholine receptor in the pathophysiology and treatment of schizophrenia. *Biochemical Pharmacology, 86*(8), 1122-1132.